Alma Mater Studiorum – Università di Bologna

DOTTORATO DI RICERCA IN

Meccanica e Scienze Avanzate dell'Ingegneria.
Disegno e Metodi dell'Ingegneria Industriale e Scienze Aerospaziali: Meccanica e Controllo del Volo

Ciclo 29º

Settore Concorsuale di afferenza: 09/A1 - Ingegneria aeronautica, aerospaziale e navale

Settore Scientifico disciplinare: ING IND/03 - Meccanica del volo

NONLINEAR APPROACHES TO ATTITUDE CONTROL USING MAGNETIC AND MECHANICAL ACTUATION

Presentata da: Encarnación Serrano Castillo

Coordinatore Dottorato **Relatore**

Nicolò Cavina **Fabrizio Giulietti**

Esame finale anno 2017

"C'è una forza motrice più forte del vapore, dell'elettricità e dell'energia atomica: la volontà."

"There is a driving force more powerful than steam, electricity and nuclear power: the will."

"Hay una fuerza motriz más poderosa que el vapor, la electricidad y la energía atómica: la voluntad."

Albert Einstein

Abstract

This thesis argues the attitude control problem of nanosatellites, which has been a challenging issue over the years for the scientific community and still constitutes an active area of research. The interest is increasing as more than 70% of future satellite launches are nanosatellites. Therefore, new challenges appear with the miniaturisation of the subsystems and improvements must be reached. In this framework, the aim of this thesis is to develop novel control approaches for three-axis stabilisation of nanosatellites equipped with magnetorquers and reaction wheels, to improve the performance of the existent control strategies and demonstrate the stability of the system. In particular this thesis is focused on the development of non-linear control techniques to stabilise full-actuated nanosatellites, and in the case of underactuation, in which the number of control variables is less than the degrees of freedom of the system.The main contributions are, for the first control strategy proposed, to demonstrate global asymptotic stability derived from control laws that stabilise the system in a target frame, a fixed direction of the orbit frame. Simulation results show good performance, also in presence of disturbances, and a theoretical selection of the magnetic control gain is given. The second control approach presents instead, a novel stable control methodology for three-axis stabilisation in underactuated conditions. The control scheme consists of the dynamical implementation of an attitude manoeuvre planning by means of a switching control logic. A detailed numerical analysis of the control law gains and the effect on the convergence time, total integrated and maximum torque is presented demonstrating the good performance and robustness also in the presence of disturbances.

Acknowledgements

My research at the University of Bologna has been influenced by a number of great professors, colleagues and friends.

Firstly, I would like to thank my thesis supervisor, Prof. Fabrizio Giulietti, for his trust and advice over the years, his support was essential for all the projects that I was involved in, throughout the period at the Flight Mechanics Laboratory. I would like to thank my colleague, Prof. Emanuele de Angelis for introducing me in the attitude control field, his support during the initial part of the PhD track was really helpful, and to Prof. Giulio Avanzini for his useful advises.

I would like to thank my supervisor during my research period at Coventry University, Prof. Nadjim Horri for his always useful support and the way he has to develop my thinking.

Throughout these 4 years, I had the opportunity to participate into different space related projects and I am honoured to thank all BEXUS (Balloon Experiment University Students) team within the BEXUS programme of the European Space Agency (ESA) education office for all that I learnt from this hands-on experience, not only from a technical point of view but also human. I am thankful to my team A5–Unibo, I am really proud of what we reached with commitment working together for the final goal to launch our experiment to the stratosphere.

I would like to thank my colleagues of the Imagine mission. It was an amazing experience to work with all of you from 11 universities and 8 different countries. I am so proud of us, who demonstrated to the National Institute of Aeronautics (NIA) and the National Aeronautics and Space Administration (NASA) that an international

team with different cultures, backgrounds and different skills can develop such a feasible, low-cost and innovative concept for a mission to the Mars system. I am glad to have had the opportunity to apply my knowledge to the AOCS (Attitude and Orbit control System) of the mission and I would like to thank the RASC-AL team for all the lessons learned, all their support and for the awards received, that are the perfect reward for all the work developed.

Last but not least, to my family, my boyfriend and my friends in Madrid, Forlì and Coventry, who have always supported me in spite of the distance.

Thank you to all of you that have walked with me throughout these four years and have contributed to making all these days of hard work an unforgettable experience.

Nani Serrano Castillo

Contents

List of Figures

Nomenclature

Symbols

$\boldsymbol{b}$	Geomagnetic field vector expressed in $\mathbb{F}_B$, T
$\hat{\boldsymbol{b}}$	Underactuated direction
C_D	Spacecraft drag coefficient
$\boldsymbol{e}, \phi$	Euler axis and Euler angle
$\hat{\boldsymbol{e}}_1, \hat{\boldsymbol{e}}_2, \hat{\boldsymbol{e}}_3$	Spacecraft principal axes of inertia
$\mathbb{F}_B$	Body-fixed frame
$\mathbb{F}_I$	Inertial frame
$\mathbb{F}_O$	Local-vertical/local-horizontal orbit frame
$\mathbb{F}_T$	Target frame
$\hat{\boldsymbol{g}}$	Non-nominal Euler axis
$\boldsymbol{g}_i$	$= (g_1, g_2, g_3)^T$Torque on the reaction-wheels, N m
$\boldsymbol{h}$	$= (h_1, h_2, h_3)^T$ Angular momentum of the wheels relative to $\mathbb{F}_B$, N m s
i	Orbit inclination, deg
$\mathbb{I}_3$	3×3 identity matrix
$\boldsymbol{I}$	Spacecraft inertia matrix, kg m^2
I_w	Moment of inertia of the momentum-wheel, kg m^2
k_ω,k_q,k_ζ	Control gains Case 1
k_ω,k_ϕ,g,k	Control gains Case 2 (Switching and Horri et al. control laws)
l_1,l_2,l_3	Spacecraft dimensions, m
$\boldsymbol{M}$	$= (M_1, M_2, M_3)^T$ External torque acting on the spacecraft, N m
$\boldsymbol{m}$	$= (m_1, m_2, m_3)^T$ Magnetic dipole moment vector, A m^2
$\boldsymbol{m}_{rm}$	Residual dipole moment, A m^2
n	Orbit rate, rad s^{-1}
$\hat{\boldsymbol{o}}_1, \hat{\boldsymbol{o}}_2, \hat{\boldsymbol{o}}_3$	Orbital axes
$\boldsymbol{p}$	$= (p_1, p_2, p_3)^T$ Modified Rodrigues parameters
$\boldsymbol{P}$	Desired attitude quaternion
$\boldsymbol{q}$	Quaternion
r_p	Gibbs vector
r_c	Orbit radius, km
T_{orb}	Orbit period, s
$\mathbb{T}_{BI}$	Coordinate transformation matrix between $\mathbb{F}_I$ and $\mathbb{F}_B$
$\mathbb{T}_{BO}$	Coordinate transformation matrix between $\mathbb{F}_O$ and $\mathbb{F}_B$
$\mathbb{T}_{BT}$	Coordinate transformation matrix between $\mathbb{F}_T$ and $\mathbb{F}_B$

$\boldsymbol{V}$	Lyapunov candidate Case 1
$\boldsymbol{V}_t$	$= (0, V_t, 0)^T$ Translational velocity along the orbit, m s^{-1}
$\mathbf{0}_{m\times n}$	$m \times n$ zero matrix
V_1 and V_2	Multiple Lyapunov functions
V_T	Common Lyapunov function for the switching approach
$\boldsymbol{Z}$	Angular momentum error expressed in the inertial frame

Greek symbols

$\boldsymbol{\epsilon}_{des}$	Threshold for the switching control law
Ω	Wheel spin rate relative to the spacecraft, rad s^{-1}
$\boldsymbol{\omega}$	$= (\omega_1, \omega_2, \omega_3)^T$ Spacecraft angular velocity vector relative to $\mathbb{F}_I$, rad s^{-1}
$\boldsymbol{\omega}^{rel}$	$= (\omega_1^r, \omega_2^r, \omega_3^r)^T$ Spacecraft angular velocity vector relative to $\mathbb{F}_O$, rad s^{-1}
ψ, ϕ, θ	Euler angles, deg
ρ	Air density, kg m^{-3}
$\hat{\boldsymbol{\sigma}}$	$= \mathbb{T}_{BO}\,(0, 1, 0)^T$ Unit vector along the orbit normal
$\boldsymbol{\zeta}$	$= (\zeta_1, \zeta_2, \zeta_3)^T$ Angular momentum error, N m s

Subscripts

$_0$	Initial condition at time t_0
$_{d,\ des}$	Desired value
$_{max}$	Maximum
$_{o,\ orb}$	Vector components in the orbit frame $\mathbb{F}_O$
$_b$	Vector components in the body frame $\mathbb{F}_B$

Abbreviations

GPS	Global Positioning System
NASA	National Aeronautics and Space Administration
ESA	European Space Agency
LEO	Low Earth Orbit
MEMS	Micro-Electro-Mechanical Sensors
COTS	Commercial Off-The-Shelf components
AOCS	Attitude and Orbit Control System
ADCS	Attitude and Determination Control System
ECI	Earth Centred Inertial reference frame
CMGs	Control Moment Gyros
MRP	Modified Rodrigues Parameters

MLF	Multiple Lyapunov Function
IMU	Inertial Measurement Unit
IGRF	International Geomagnetic Reference Field
ESEO	European Student Earth Orbiter
MT	Magnetorquer
MW	Momentum Wheel
RW	Reaction Wheel
ISS	International Space Station

Chapter 1

Introduction

1.1 Attitude control in Low Earth Orbit

The attitude control of a spacecraft is the control of its orientation in space and the rotational motion about the centre of mass. The attitude and orbit are often interdependent concepts but their study has been separated over the years. Attitude in turn, is divided into determination, prediction and control [1].

- Attitude determination: Compute the orientation involving different sensors. These can be magnetometers, Sun Sensors, Earth Sensors, Star-Trackers and GPS, which can be combined to achieve the required accuracies of the mission. The most common used sensors are sun sensors and magnetometers.
- Attitude prediction: The process of forecasting the future orientation using the previous attitude information, algorithms and dynamical models which include the applied and environmental torques.
- Attitude control: Is the process to keep the orientation or reach a new desired orientation. Using the actuators available to stabilise the attitude, correcting

the internal and external perturbations respect to a desired target attitude.

This thesis will be focused on the attitude control problem of small and nanosatellites orbiting in Low Earth Orbit (LEO).

Over the years, the number of space missions has increased whereas mission architectures have been reduced in size and mass. Important International space agencies such as the National Aeronautics and Space Administration (NASA) and the European Space Agency (ESA), started increasing programmes based on smaller satellites with simpler architectures, which was possible due to the encouraging development of Micro-Electro-Mechanical Sensors (MEMS) and Commercial Off-The-Shelf components (COTS). Electrical power, fuel consumption, and payload mass and dimension were reduced as well as new attitude and orbit determination and control Systems.

In 1999 the CubeSat Standard was defined with the aim to provide design guidelines for the interface between the launch vehicle and the spacecraft, which allow developers to pool together for launch, reducing costs, and creating opportunities [2]. Since then, CubeSats have been built not only by universities but also by commercial companies and international space agencies, due to their simplicity in design, architecture, and objective, and the possibility to purchase smaller space-qualified subsystems at affordable prices.

This new trend represents a challenge in the miniaturization of all of traditional subsystems. Data-handling and power systems technologies are quite advanced but the open issues in attitude control performance are yet present. These are focused on dynamic control and control accuracies which are related to other satellite subsystems as the communication, data-handling, thermal and power.

Different attitude determination and control strategies have been developed. Typical constraints posed on small satellites in terms of mass, volume, and available power usually resulted in a pointing accuracy that has to compete with bigger platforms. It is essential to enhance such strategies both relying on hardware improvement and novel results in control theory.

Attitude control methods can be classified in active and passive:

- Passive control: They do not need any input or feedback, they take advantage of natural physical effects.
  - Spin stabilised systems.
  - Dual-spin stabilised systems.
  - Stabilisation by gravity gradient.
  - Stabilisation by bias-momentum stabilised systems.
  - Stabilisation by magnetic moments
- Active control: They operate by taking an error signal an require a continuous actuation from control devices.

The attitude control system of a satellite depends on the type mission, stability and pointing requirements, power and mass constraints, orbit characteristics, and total mass.

Most satellites, the International Space Station, and the Hubble Space Telescope are all in Low Earth Orbit (LEO). As main features, these orbits are from $200 - 2000km$ having a mean orbital velocity of $7.8km/s$. This type of orbit is one of the

most convenient for Earth observation and to study the space environment effect in humans as the time to reach the orbit is relatively short.

An important feature of this orbit is the presence of some atmospheric drag which over time will slow down the satellite whose orbit slowly decay. This allows the influence of gravity to pull the object towards the Earth. Other fact is related to how quickly a satellite in LEO goes around the Earth.

The market of nanosatellites is increasing for commercial and educational purposes for satellites to LEO due to the simpleness and cheapness of the missions [3] although the number of launches has been reduced since 2014 due to delays in mission phases, 2017 will probably be a record year as these delayed nanosatellites will be probably launched throughout the year.

LEO satellites offer not high coverage and dwell time over a certain region. However, they offer very good bandwidth for communications and represent a good platform for remote sensing if the attitude and orbit control system (AOCS) can reach the pointing requirements. Regarding the accuracy obtained by these control systems, there are still many open issues.

The purpose of this thesis is to give a contribution on the enhancement of the AOCS, by focusing on three-axis stabilisation strategies for nanosatellites, to improve the existent approaches in terms of performance and stability.

1.2 Outline of the thesis

This thesis is divided in two main parts, the first three chapters give an overview of AOCS for nanosatellites in LEO, highlighting the problem of three-axis control. The

second part corresponds with my personal contributions to the scientific community followed by the conclusions.

In Chapter 1 an introduction to attitude control for small satellites in low Earth Orbit is given.

Chapter 2 describes the mathematical model of the satellite, the parameters needed for attitude representation followed by an overview of the disturbances in LEO environment and a description of the most common AOCS actuators.

Chapter 3 gives a brief summary of three-axis attitude control for this class of satellites and a description of the underactuation problem.

Two results are presented in the following chapters, namely Case 1 and Case 2:

In chapter 4, a three-axis control of a spacecraft using both magnetic and mechanical actuation is presented. Three reaction wheels are used to control the spacecraft attitude, and three magnetic torque rods are used for continuous autonomous momentum dumping. A proof of global asymptotic stability is derived for control laws that stabilise the cascade system in the target frame, a fixed direction of the orbit frame. Good performance, also in presence of disturbances, is shown in simulations and a theoretical selection of the magnetic control gain is given.

In Chapter 5, a novel stable control methodology for three-axis stabilisation of a nanosatellite in underactuated conditions is developed in which just two independent torque components are given by two reaction wheels. The control approach proposed tracks angular velocities by means of a switching control logic. A detailed numerical analysis of the control law gains and their effect on the convergence time, total integrated and maximum torque is presented. Numerical simulations of existing

and proposed control laws are given to show attitude asymptotic stabilisation of the satellite using the proposed switching control law. Robustness in presence of disturbances is shown followed by the description of the enhancements respect to a previous controller.

Main conclusions and the possible future work end the thesis.

Chapter 2

Mathematical model and description of the satellite in LEO environment

In this chapter, the attitude control system of the satellite will be described, including the elements used analytically to represent the attitude. Actuators and the mathematical model will be presented as well as the disturbances in LEO environment.

2.1 Attitude representation

2.1.1 Reference frames

In order to represent the motion of an Earth-orbiting rigid satellite and the space environment effects the following reference frames are introduced.

1. A local-vertical/local-horizontal orbital frame, named $\mathbb{F}_O$. The origin of this

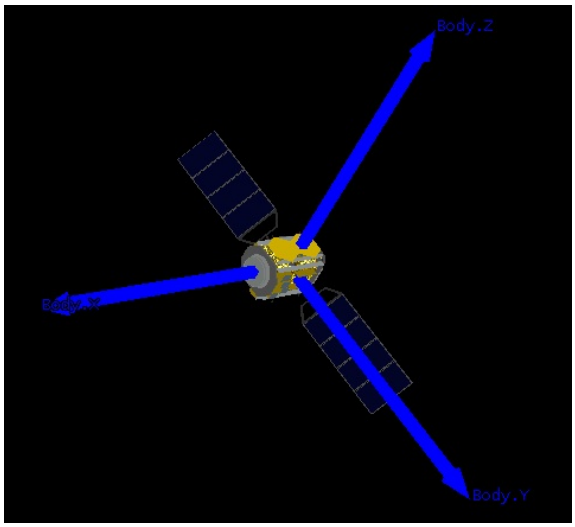

Figure 2.1: Body-axis reference frame

frame coincides with the centre of mass of the satellite. It rotates relative to the ECI frame, with a rate of $\boldsymbol{\omega}_O^{orb}$ or orbital angular velocity, depending on the radius of the orbit. The x_o axis points in the direction of motion tangentially to the orbit. For a circular orbit, x_o is parallel to the direction of the orbital velocity. The Z-axis of the frame points towards the centre of the Earth, and the y_o axis completes the right hand system.

2. A body-fixed frame $\mathbb{F}_B$. Its origin is placed in the center mass of the satellite. The nadir side of the satellite is in the z_b direction, and the other two axes, x_b and y_b, are coincident with x_o and y_o of the orbit frame when the satellite has an attitude of zero degrees in roll, pitch and yaw.

3. The Earth-Centred Inertial (ECI) $\mathbb{F}_I$, whose origin is at the Earth's centre, the x_I axis is the vernal equinox direction, the z_I axis coincides with Earth rotation axis and it is northward directed, and the y_I completes an orthogonal right-handed frame. For Earth orbiting spacecraft problems $\mathbb{F}_I$ is an inertial frame.

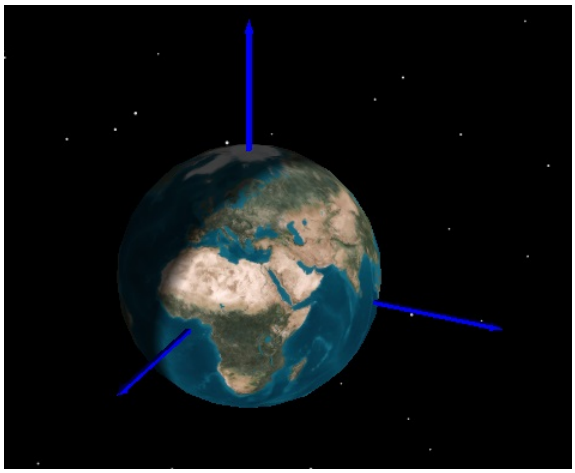

Figure 2.2: Earth-Centred Inertial reference frame

4. A target frame, $\mathbb{F}_T$, which denotes the spacecraft desired attitude. Also, for the purposes of this thesis, the target frame, $\mathbb{F}_T$, is constant with respect to the orbital frame, $\mathbb{F}_O$.

2.1.2 Attitude Parametrization and Kinematics

This section highlights different representations of a satellite attitude.

- **Euler angles**

  Any rotation is expressed as a sequence of elementary rotations.

  A rotation is an angle ψ about the z-axis, the second rotation is an angle θ about the y-axis, and the third rotation is an angle ϕ about the x-axis. For notational brevity, let us arrange these angles in a three-dimensional vector called the Euler angle vector $\boldsymbol{E}$, defined by

$$\boldsymbol{E} := [\phi, \theta, \psi]^T$$

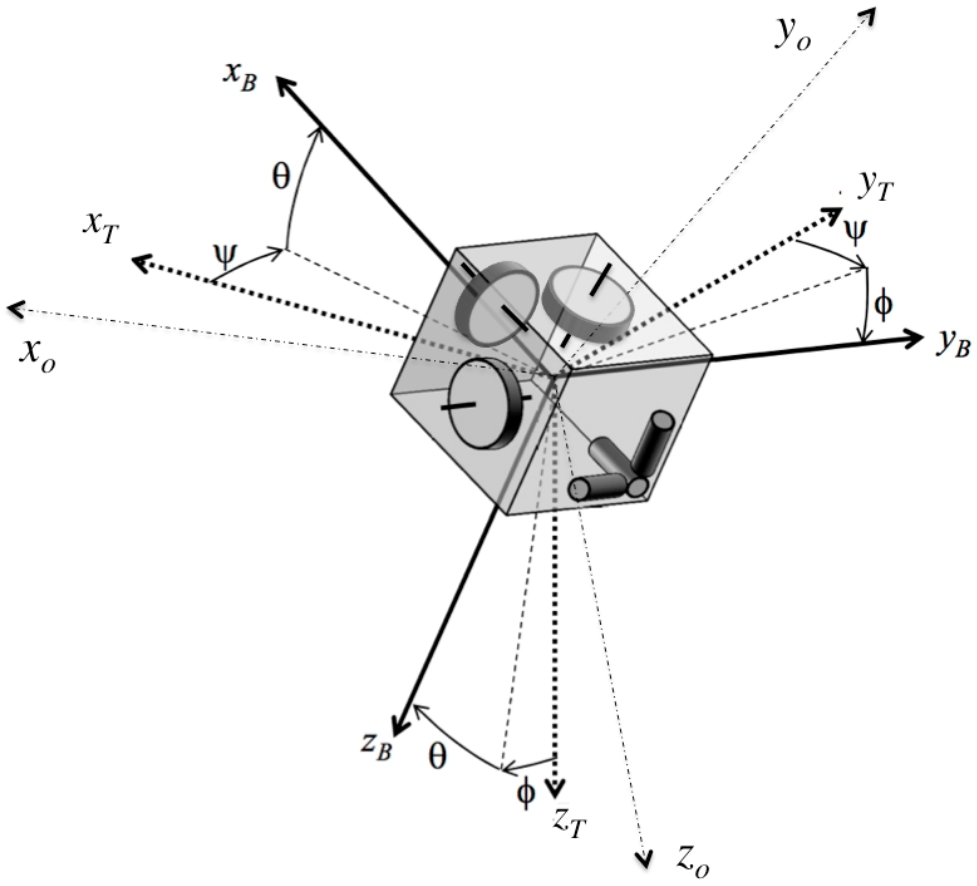

Figure 2.3: Small satellite equipped with three RWs and three MTs

The final direction cosine matrix can be expressed as multiplication of the successive rotations.

$$R_{ijk}(\phi, \theta, \psi) := R_i(\phi) R_j(\theta) R_k(\psi)$$

In this thesis, the "yaw" angle ψ around the local vertical z_O is given by the angular distance between the y_O-axis and the projection of y_B on the orbit plane, whereas the "roll" angle ϕ is represented by the elevation of y_B with respect to the orbit plane. The sequence of fundamental rotations is completed

by a "pitch" rotation θ around the unit vector $\hat{\boldsymbol{e}}_2$, parallel to y_B, as represented in Fig. 2.3.

The attitude of the spacecraft with respect to $\mathbb{F}_O$ can be described by different sequences, for a 3-1-2 Euler angle sequence, the matrix is

$$\boldsymbol{T}_{BO} = \begin{pmatrix} \cos\psi\cos\theta - \sin\phi\sin\psi\sin\theta & \cos\theta\sin\psi + \cos\psi\sin\phi\sin\theta & -\cos\phi\sin\theta \\ -\cos\phi\sin\psi & \cos\phi\cos\psi & \sin\phi \\ \cos\psi\sin\theta + \cos\theta\sin\phi\sin\psi & \sin\psi\sin\theta - \cos\psi\cos\theta\sin\phi & \cos\phi\cos\theta \end{pmatrix} \tag{2.1}$$

The evolution of Euler Angles is a function of the angular speed of the spacecraft relative to $\mathbb{F}_O$, given by $\boldsymbol{\omega}^{rel} = \boldsymbol{\omega} - \boldsymbol{T}_{BO}\,\boldsymbol{\omega}_O^{orb}$, where $\boldsymbol{\omega}_O^{orb} = (0, n, 0)^T$ is the angular speed of $\mathbb{F}_O$ with respect to an inertial frame $\mathbb{F}_I$, with components expressed in $\mathbb{F}_O$ [4].

The kinematics of Euler Angles (yaw, roll, and pitch) written as a function of the angular speed of the spacecraft relative to $\mathbb{F}_O$,

$$\omega_1^{rel} = \dot{\phi}\cos\theta - \dot{\psi}\cos\phi\sin\theta \tag{2.2}$$

$$\omega_2^{rel} = \dot{\theta} + \dot{\psi}\sin\phi \tag{2.3}$$

$$\omega_3^{rel} = \dot{\phi}\sin\theta + \dot{\psi}\cos\phi\cos\theta \tag{2.4}$$

which in terms of absolute angular velocity vector of the satellite $\boldsymbol{\omega} = \boldsymbol{\omega}^{rel} + \boldsymbol{T}_{BO}\,\boldsymbol{\omega}_O^{orb}$:

$$\omega_1 = \dot{\phi}\cos\theta - \dot{\psi}\cos\phi\sin\theta + n\,(\cos\theta\sin\psi + \sin\phi\sin\theta\cos\psi) \tag{2.5}$$

$$\omega_2 = \dot{\theta} + \dot{\psi}\sin\phi + n\,\cos\phi\cos\psi \tag{2.6}$$

$$\omega_3 = \dot{\phi}\sin\theta + \dot{\psi}\cos\phi\cos\theta + n\,(\sin\theta\sin\psi - \sin\phi\cos\theta\cos\psi) \tag{2.7}$$

For this type of attitude representation by a sequence of elementary rotations, a notable characteristic is that singular configurations occur [5]. Both classical yaw-pitch-roll (3-2-1) and precession-nutation-spin (3-1-3) sequences will approach singular configurations. All parametrizations of the form (i, j, i), that there exists a singularity at the home position, $[\phi, \theta, \psi] = [0, 0, 0]$. The singularities found in the various Euler angle representations are said to arise from gimbal-lock which may be understood in several ways. Intuitively, it arises from the indistinguishably of changes in the first and third Euler angles when the second Euler angle is at some critical value.

Practical applicability of a certain control law and the search closed-loop stability proofs motivate the recommendation of this unusual Euler angle sequence in the description of spacecraft attitude kinematics if Euler Angles are chosen for attitude parametrization.

- **Euler Axis-Angle $(\boldsymbol{e}, \phi)$**

  Euler axis-angle represents a nominal rotation which takes a rotating reference frame (e.g., a body-fixed frame) to a target reference frame by means of the minimum angular path. It is often used for commanding slew manoeuvres [6]. The Euler axis is represented by $\boldsymbol{e}$ and the Euler angle by ϕ. The kinematics of both are described by

$$\dot{\boldsymbol{e}} = \frac{1}{2}\left[\boldsymbol{e}^{\times} - \cot\frac{\phi}{2}\,\boldsymbol{e}^{\times}\,\boldsymbol{e}^{\times}\right]\boldsymbol{\omega} = \boldsymbol{E}(\phi)\boldsymbol{\omega} \tag{2.8}$$

$$\dot{\phi} = \boldsymbol{e}^{T}\,\boldsymbol{\omega} \tag{2.9}$$

  where "*cot*" is the cotangent of the angle, $\boldsymbol{e}^{x}$ is the skew-symmetric matrix and $\boldsymbol{\omega}$ is the angular velocity.

  In some cases, there exist a direction about which rotations are not allowed, being the nominal Euler transformation not attainable. Nonetheless, rotations

about non-nominal axes, on the plane orthogonal to the forbidden direction, can be performed [7].

The non-nominal Euler axis $\hat{\boldsymbol{g}}$ is represented as

$$\hat{\boldsymbol{g}} = (\hat{\boldsymbol{b}} \times \hat{\boldsymbol{e}})/\|\hat{\boldsymbol{b}} \times \hat{\boldsymbol{e}}\| \tag{2.10}$$

and it is also called the admissible rotation eigenaxis.

- **Quaternions**

  Quaternions are a very efficient way to represent the attitude. Having four parameters and being free of singularities [8]. Although they have no physical representation, its geometric meaning can be trivially recovered. The quaternion algebra allows to easily compose rotations.

  A quaternion can be represented by $\boldsymbol{q} = [cos(\phi) + \boldsymbol{e}_i sin(\phi)]$ where $\boldsymbol{q} = [q_1, q_2, q_3, q_4]^T = [\bar{\boldsymbol{q}}^T, q_4]^T$ $\bar{\boldsymbol{q}}^T$ is the quaternion vector and $\boldsymbol{e}_i$ the components of the Euler Axis

$$\begin{aligned} q_1 &= \boldsymbol{e}_1 sin(\phi/2) \\ q_2 &= \boldsymbol{e}_2 sin(\phi/2) \\ q_3 &= \boldsymbol{e}_3 sin(\phi/2) \\ q_4 &= cos(\phi/2) \end{aligned}$$

  The kinematics can be represented by

$$\dot{\boldsymbol{q}} = \boldsymbol{W}(q)\,\boldsymbol{\omega} \tag{2.11}$$

$$\boldsymbol{W}(q) = 1/2\,(q_4\,\mathbb{I}_3 + \bar{\boldsymbol{q}}^{\times} - \bar{\boldsymbol{q}}^T)^T \tag{2.12}$$

being $\bar{\boldsymbol{q}}^{\times}$ the skew-symmetric matrix.

This expression can also be represented by

$$\dot{\boldsymbol{q}} = \frac{1}{2}(q_0\boldsymbol{\omega} + \boldsymbol{q}^x\boldsymbol{\omega}) \tag{2.13}$$

$$\dot{q_0} = -\frac{1}{2}\boldsymbol{q}^T\,\boldsymbol{\omega} \tag{2.14}$$

Quaternions present several advantages over Euler angles, above all the absence of inherent geometric singularity. Moreover, the linear equation which determine their evolution as a function of angular velocity components is less computationally expensive than that derived for the Eulers angles.

The four parameters are not independent and must satisfy the constraint

$$q_1^2 + q_2^2 + q_3^2 + q_4^2 = 1 \tag{2.15}$$

Quaternions will be the attitude representation selected for the control approaches described in this thesis.

- **Gibbs Vector**

  Attitude representation in terms of quaternions has a non-minimality which can be solved for by use of the Gibbs vector,

  $$\boldsymbol{r}_p = (r_{p1}, r_{p2}, r_{p3})^T = atan(\hat{\alpha}/2) \tag{2.16}$$

  Gibbs parameters, also known as Rodrigues parameters, and are strictly related to quaternions. Being a minimal parametrization of attitudes. They present a singularity.

  The singular configuration of the Gibbs vector is for any eigenaxis rotation with $\alpha = \pm\pi$, in which case their values diverge towards infinity. To solve

for this problem, the Modified Rodrigues parameters (MRP) were recently introduced, defined as

$$\boldsymbol{p} = (p_1, p_2, p_3)^T = atan(\hat{\alpha}/4) \tag{2.17}$$

The singularity in the attitude representation is still present, and placed at half of a rotation (that is, $\alpha = \pm\pi$). Nonetheless, an advantage is that they do not diverge. All these features make the numerical integration of MRPs less critical with respect to both the quaternions case and the Gibbs vector.

2.2 Mathematical model

A satellite platform will be considered a rigid body in the space and its attitude changes according to the fundamental equations for rotational dynamics,

$$\boldsymbol{I}\,\dot{\boldsymbol{\omega}} + \dot{\boldsymbol{h}} + \boldsymbol{\omega} \times (\boldsymbol{I}\,\boldsymbol{\omega} + \boldsymbol{h}) = \boldsymbol{M} \tag{2.18}$$

where $\boldsymbol{\omega} = (\omega_1, \omega_2, \omega_3)^T$ is the absolute angular velocity vector of the satellite with respect to $\mathbb{F}_I$, $\boldsymbol{I} = diag\,(I_1, I_2, I_3)$ which is the spacecraft inertia matrix. The term $\boldsymbol{h} = (h_1, h_2, h_3)^T$ is the angular momentum vector relative to $\mathbb{F}_B$ of any rotational momentum exchange devices such as, RWs, CMG's or thrusters.

Eq.(2.18) shows that the magnitude of angular momentum in a system can only be changed by applying external torques, because the change due to the term $\boldsymbol{\omega} \times (\boldsymbol{I}\,\boldsymbol{\omega} + \boldsymbol{h})$ can only change the direction, not the magnitude.

Eq.(2.19), represents the total momentum vector $\boldsymbol{M} = (M_1, M_2, M_3)^T$, which includes external disturbances, $\boldsymbol{M}^{(d)}$, and magnetic control, $\boldsymbol{M}^{(c)} = \boldsymbol{m} \times \boldsymbol{b}$, being $\boldsymbol{m} = (m_1, m_2, m_3)^T$ the magnetic dipole moment vector. See section 2.2.1.4.

$$\boldsymbol{M} = \boldsymbol{M}^{(c)} + \boldsymbol{M}^{(d)} \tag{2.19}$$

In the most general case, the relative angular momentum of a rotational device such as a reaction wheel, $h = I_w\Omega$, where I_w is the moment of inertia of the wheel about its spin axis $\hat{\boldsymbol{a}}$, and Ω is the wheel spin rate with respect to the spacecraft. Therefore, one obtains

$$\dot{h_i} = \boldsymbol{g}_i - I_w\, \dot{\boldsymbol{\omega}}^T \hat{\boldsymbol{a}}_i \tag{2.20}$$

where $\boldsymbol{g}_i$ is the torque applied to the wheel about its spin axis by its electric motor. In the ideal case when the wheel assembly is not affected by friction, $\boldsymbol{g}_i$ represents the control input.

Regarding orbital parameters considered for this thesis, a circular LEO of radius r_c, period T_{orb}, and orbit rate $n = 2\pi/T_{orb}$.

2.2.1 External disturbances

As AOCS subsystem must ensure the correct orientation in space, it has to counteract the perturbations in the form of disturbance torques and forces that modify the nominal trajectory and attitude of satellite [9].

For a LEO orbit, the most important environmental disturbances are:

- Gravity Gradient

- Solar radiation pressure
- Atmospheric Drag
- Magnetic field and residual dipole

2.2.1.1 Gravity gradient torque

A non-symmetrical object in orbit is subject to a gravitational torque because of the variation in Earth's gravitational force over the object. This gravity-gradient torque results from the inverse square gravitational force field. It is constant for Earth-oriented; cyclic for inertially oriented. When one of the principal axis is aligned with the local vertical, the *cg* is always on that principal axis, and therefore there is no gravity gradient torque. It increases with the angle between the local vertical and the spacecrafts principal axes, always trying to align the minimum principal axis with the local vertical. An expression for the gravity gradient torque for a spacecraft with the minimum principal axis in its Z direction is given by

$$\boldsymbol{M}^{(gg)} = 3n^2 \left[\hat{\boldsymbol{o}}_3 \times (\boldsymbol{I}\hat{\boldsymbol{o}}_3)\right] \tag{2.21}$$

where $\hat{\boldsymbol{o}}_3$ is the unit vector parallel to the local vertical, n the orbit rate and $\boldsymbol{I}$ the inertia matrix.

Gravity gradient can be used as a passive form of stabilisation, as well as a simple momentum desaturation technique. However, for stabilisation, it is highly susceptible to other environmental disturbances.

2.2.1.2 Aerodynamic torque

The interaction of the upper atmosphere molecules with the external surface of the satellite introduce. The aerodynamic torque is the dominant disturbance torque below approximately 400 km. It is possible to assume that the incident particles entire energy is absorbed on collision. This is modelled as an elastic impact without reflection.

Aerodynamic torque is thus equal to

$$\boldsymbol{M}^{(a)} = \boldsymbol{r}_{cp} \times \boldsymbol{F}^{(a)}$$

where $\boldsymbol{r}_{cp}$ is the position of the centre of pressure with respect to the centre of mass of the satellite, and $\boldsymbol{F}^{(a)} = (1/2)\rho V_t^2 A C_D$ is the aerodynamic force produced by the rarefied air with density $\rho \approx 3.614 \cdot 10^{-14}$ kg/m^3, at the considered orbit altitude. In the expression of $\boldsymbol{F}^{(a)}$, A is the cross-sectional area, V_t is the velocity with respect to the air, assumed equal to the orbital speed, and C_D is a drag coefficient. It can be calculated as the vector sum of the individual torques given by the cross product of the vector joining the spacecraft centre of mass to the centre of pressure of each geometric shape times the force acting on the component.

2.2.1.3 Solar radiation pressure

The solar radiation has momentum, and therefore it exerts pressure on those objects it strikes. The radiation incident on a spacecraft's surface produces a force which results in a torque about the spacecraft's centre of mass. It is cyclic for Earth-oriented satellites and constant for Sun-Oriented ones.

The major factors determining the radiation torque on a spacecraft are the intensity and spectral distribution of the incident radiation, the geometry of the surface and its optical properties, and the orientation of the Sun vector.

Sources of electromagnetic radiation pressure can be the solar illumination, the reflection of the radiation by the Earth and its atmosphere and the radiation emitted from the Earth and its atmosphere.

The torque produced can be represented as

$$T_s = \frac{F_s}{c} A_s (1+q)(cp_s - cg)cos(i) \tag{2.22}$$

where Fs is the solar constant 1367 W/m2, c is the speed of light, $3 \cdot 10^8 m/s.$, A_s the surface area of the satellite facing the sun, q is the reflectance factor, i is the angle of incidence to the sun, cp_s is the location of the centre of solar pressure, and cg is the centre of gravity.

2.2.1.4 Magnetic field and residual magnetic dipole

The Earths liquid core generates the Earths magnetic field. Some features are that it is complex, asymmetric and not aligned with Earths spin axis, and varies both with gravitational movement of the dipole and changes in solar particle flux. However, for the use in the AOCS design process, it is usually sufficient to model the Earth's magnetic field as a dipole and to determine the maximum possible value of the magnetic torque for a satellite orbit.

On-board electrical systems and circuits can generate a dipole moment $\boldsymbol{m}_{rm}$ which can produce residual magnetic torque $\boldsymbol{M}^{(rm)}$. When the residual moment of a satellite is not aligned with the Earth's Magnetic field, the torque generated

attempts to align the magnet to the local field. The residual dipole moment is relatively negligible when magnetic coils are active, when they are switched off, it produces a significant contribution to the disturbance torque that is described by

$$\boldsymbol{M}^{(rm)} = \boldsymbol{m}_{rm} \times \boldsymbol{b} \tag{2.23}$$

The primary sources of magnetic disturbance torques are: (1) Spacecrafts magnetic moments (2) Eddy currents (3) Hysteresis These residual moments can range from 0.1 to 20 Am^2 depending on the satellite size and whether any on-board compensation is provided.

The components of the geomagnetic field in the model are provided in the local-vertical/local-horizontal orbit frame, $\mathbb{F}_O$, by means of the International Geomagnetic Reference Field (IGRF) model [10]. This model represents the set of gaussian coefficients for use in the analytical models describing the Earth's magnetic field and is updated every five years.

2.2.2 Actuators for attitude control of small and nanosatellites in LEO

Actuators will provide the satellite with the torque needed to detumble the satellite after the release from the launch vehicle, to perform slew manoeuvres, to point a target direction or to keep a desired attitude [9]. In the case for small and nanosatellites it is still a challenge as although the inertia is low, which means less torque required than bigger satellites to perform the same manoeuvre. Reliability and quality of smaller actuators that can fit in these satellites are still being developed.

The most common attitude actuators for nanosatellites in LEO are summarized this section 2.2.2. They are divided into momentum-exchange devices which con-

serve angular momentum in the spacecraft: reaction/momentum wheels and control moment gyros. And the external torque actuators, which change the angular momentum of the spacecraft when they are activated, such as magnetorquers and thrusters (cold-gas, hot-gas and electric)

Some pico-satellites are launched without any attitude control system. But normally missions require attitude control methods. In LEO, both active or passive methods are used. Spin-stabilisation and a gravity gradient are two examples of simple and effective means of attaining a certain attitude but the most common actuators for small-class satellites are the momentum exchange devices, suitable for more precise control. [11].

2.2.2.1 Thrusters

Thrusters are possibly the most frequently flown attitude actuator. They are used for orbital manoeuvres, rapid slews, and in many cases, some subset of the thrusters used is for attitude control and managing angular momentum. They generate a force by expelling propellant at high-velocity from their exit nozzles and provide a torque proportional. Types and other features are described in Table 2.1.

2.2.2.2 Mechanical control

Mechanical control is given by rotating masses within the satellite body. These are angular exchange devices in which the angular momentum is transferred between different parts of the satellite. See Table 2.2 and Table 2.3

For fast, accurate maneuvers attitude reaction wheels can be chosen, since they

Table 2.1: Thrusters

Thrusters	Description
Types	• Hot-gas propulsion systems include thrusters that chemically alter the propellant to extract the energy needed for rapid mass expulsion. Monopropellant: The propellant is catalysed o break down chemically. Bi-propellant: In which a fuel is mixed with an oxidizer to achieve combustion just prior to expulsion. • Cold-gas systems include thrusters whose propellant is not altered chemically during propulsion. The energy may come from phase change of the propellant, or simply from the pre-pressurising the propellant in its tank. • Electrical propulsion: It is accomplished by using magnetic or electrostatic fields to eject plasma o magnetic fluid to achieve a reaction force on the spacecraft.
Advantages	They are able to provide large, instantaneous control torques at any time in the orbit.
Disadvantages	They use expendable propellant. They can disrupt orbit determination activities, and the expelled matter can impinge on the surface of the spacecraft, possibly heating or contaminating surfaces.

Table 2.2: Wheels

Wheels	Description
Types	• Reaction Wheels: They are essentially torque motors with high-inertia rotors. They can spin in either direction and provide one axis of control for each wheel. They store momentum. Nominal velocity is zero. • Momentum wheels are reaction wheels with a nominal spin rate not zero to provide a nearly constant angular momentum. This momentum provides gyroscopic stiffness to two axes, and the motor torque may be controlled to change pointing around the spin axis. In sizing wheels we must always consider two performance quantities: angular momentum capacity, and torque authority.
Advantages	Provides smooth changes in torque, allowing very accurate pointing of spacecraft.
Disadvantages	Some wheels can cause vibrations, or jitter, at high speeds, but this can often be mitigated with vibration isolators of changes in structural design.

permit a smooth and continuous control with the minimum possible parasitic disturbances. The levels achievable are typically ranging from 0.01 to 2 Nm.

2.2.2.3 Control moment gyros (CMGs)

These are single-or double-gimbaled wheels spinning at constant speed and therefore providing momentum bias stiffness when not actuating. By turning the gimbal axis, it can be obtained high-output torque whose size depends on the speed of the rotor the gimbal rate of rotation. They can be achieved with levels about 200 Nm. However, such devices are very heavy and are rarely used in the system attitude control of satellites ordinary size.

Table 2.3: CMG's

CMG's	Description
Advantages	For high torque applications in which fine control is needed, control moment gyros maybe used instead of reaction wheels. Control systems with two or more CMGs can produce large torques about all three orthogonal axes of the spacecraft, thus we most often use them where agile (i.e. high angular rate) manoeuvres are required.
Disadvantages	The use of CMGs requires complex control laws and careful momentum management to avoid wheel saturation. Also, because the CMGs torque is created by twisting what is essentially a stiff gyroscope perpendicular to its Spin axis, the bearings of the wheel suffer a great deal of wear and tear, causing most CMGs to have shorter lifetimes than other actuators. Because CMGs combine a short life with high cost, weight, and power needs, they are generally used only on very large spacecraft and only when necessary to achieve the mission goals.

Normally three reaction wheels are used to control the spacecraft, arranged with wheels aligned with the principal axes of the vehicle; is common also add a fourth reaction wheel for redundancy.

2.2.2.4 Magnetorquers

Magnetorquers (MTs) consist of current-driven coils (electromagnets) rigidly placed designed to generate a magnetic dipole moment. When three orthogonal torquers are mounted to a spacecraft, they can create a magnetic dipole at any direction.

A MT produces a torque which lies on a plane which is perpendicular to the Earths magnetic field vector $\boldsymbol{b}$ due to the interaction between the local geomagnetic field and the coils. The control torque is constrained to belong to that plane. Thus,

Table 2.4: Magnetorquers

MT's	Description
Advantages	Electromagnets have the advantage of no moving parts, requiring only a magnetometer for sensing and wire coiled around a metallic rod in each axis. Low cost, simplicity and effectiveness. Magnetic control systems provide a continuous and smooth control pair.
Disadvantages	Because they use the Earths natural magnetic field, and this field reduces in strength with the cube of distance from Earths centre, magnetic torquers are less effective at higher orbits. The moment levels reached by magnetorquers are small (on the order of 1-10 mNm), usually do not allow rapid manoeuvres.

the system is not capable to provide three independent control torques at each time instant. See section 3.3.

MTs are mostly used to compensate for spacecraft residual magnetic field or attitude drift from minor disturbance torques and to desaturate momentum exchange devices. Although they require more time than other actuators such as thrusters, they are commonly used due to their low cost, simplicity and effectiveness. In table 2.4, advantages and disadvantages of this actuators are presented.

Other way a satellite can control its magnetic moment is the use of gymballed permanent magnets. For three-axis control, the permanent magnet must be capable of rotating in three axes Or equivalently, three permanent magnets must be mounted on rotation-control motors with mutually non-parallel axes.

2.2.3 Momentum management

Momentum management is the process to remove the momentum stored in the satellite by the momentum exchange devices. This build-up is caused by the environmental external torques which can be cyclic or secular. Cyclic disturbances, that vary over the course of an orbit but have a mean of zero may be managed just through storage. However, secular torques which are those that have a non-zero mean, will cause a gradual increase in angular momentum [12].

Reaction wheels, which work nominally zero angular momentum, can be used primarily to absorb cyclical disturbing moments. However, the storing capacity is limited and reaction wheels can saturate reaching the maximum angular velocity. The process to remove the momentum can be periodic, as traditionally, or continuous as recent results of new control strategies show [13]. In chapter 4 the control law strategy proposes a continuous momentum dumping.

As design requirements, the average disturbance torque for 0.25 or 0.5 orbit determines the minimum, capacity of the wheels. To determine it, cyclic and secular disturbances in the spacecrafts environment must be distinguished. The size of the reaction wheels are such that to be able to store the full cyclic component of momentum without the need of momentum downloading.

Chapter 3

Three axis stabilisation for nanosatellites

3.1 Spin and three axis Stabilisation

Once a satellite is released from a rocket or from other platforms such as the space station (ISS) [14, 3] and is placed into a stable orbit, attitude must be also stabilised. Two techniques to achieve this goal will be described, namely, spin and three-axis stabilisation.

Spin stabilisation

The entire satellite rotates around an axis, spinning and keeping the satellite attitude in space under control. The spinning spacecraft resists perturbing forces due to the gyroscope effect. An advantage is the simplicity to keep the pointing to a target direction. However, instruments or antennae must "de-spin" to point certain directions and as a consequence some constraints are introduced, such as the limited use of large solar arrays.

Spin stabilisation was used for recent small and nanosatellite missions [15]. See table 3.1.

On the other hand, three-axis stabilisation allows the satellite to point a certain direction without spinning. In order to do so, satellites use different actuators to keep the satellite pointing to the desired orientation. While attitude determination sensors detect any variation of the satellite out of the proper orientation, the spinning wheels speed up or slow down to return the satellite to its correct position. Thrusters can also be used to keep the satellite within a range of allowed positions. An advantage of three-axis stabilisation is that in order to fulfil the instruments pointing requirements, "de-spin" manoeuvres are not needed.

3.1.1 Three-axis stabilisation configurations

Different momentum based ACS configurations are used for three-axis stabilised satellites [16]. Some recent small and nanosatellite missions [15] are described in table 3.2. The most common configurations are:

- Single momentum wheel.
- Pitch momentum wheel/thruster.
- Single-gimbal momentum wheel.
- Pitch momentum wheel/yaw reaction wheel.
- Double-gimbal momentum wheel.
- Three reaction wheels.

Table 3.1: Small and nanosatellites Spin Stabilised

Nanosatellites	Description
HIT-Sat(2009) Institute of Technology and Hokkaido University, Hokkaido, Japan	HIT-Sat (3 kg) is a CubeSat. The spacecraft is spin-stabilised, pointing into the sun direction. The ACS (Attitude Control Subsystem) consists of three magnetic torquers (MTQ, total mass of 90 gram) as actuators, a magnetometer (Honeywell HMC2003), a sun sensor (FOV 45) and a gyroscope (range of 200/s). A special separation system was developed for spacecraft deployment. After the separation, the initial attitude of the satellite is acquired thorough three control phases: de-spin, spin-up and sun acquisition (spin about the y-axis). The purpose of the attitude control is to stabilise the spin axis to the sun within a margin of about 10.
ANUSat(2009), Anna University of Chennai, Madras, India, and ISRO	Spin-stabilisation is provided by a pair of of magnetic torquers as actuators. Attitude sensing is provided by a 3-axis magnetometer and a twin slit sun sensor ($75deg$ range with $0.5deg$ resolution). Passive thermal control is employed. The spacecraft is spin stabilised with the spin axis orientation towards orbit normal with a pointing accuracy of $3deg$. The nominal spin rate is around 4 rpm. The spacecraft mass is 38 kg.
SNOE(1998), small satellite student project of the University of Colorado (CU) at Boulder	The satellite is spin stabilised at a spin rate of 5 rpm with the spin axis normal to the orbit plane. Attitude knowledge is provided by horizon crossing indicators, and magnetometers; attitude control is done with torque rods and nutation dampers. Mass=115kg
ELFIN (planned for November 2017)is a 3U CubeSat mission under development by the Earth, planetary, and Space Sciences department at UCLA (University of California Los Angeles).	Spin-stabilised 3U CubeSat at 20 rpm.Two torquer coils, comprised of aluminium wire on plastic spools, provide spin and precession capability to ELFIN. Periodic (daily/weekly) scheduled manoeuvres are executed with these coils using on-board control laws and a magnetoresistive magnetometer.

MicroMAS (2014)(Massachusetts Institute of Technology/Lincoln Laboratory), MIT/SSL (Space Systems Laboratory) and the University of Massachusetts at Amherst.	The ADCS (Attitude Determination and Control Subsystem) uses the x reaction wheel primarily to cancel out the angular momentum of payload scanner assembly. It operates in a dual-spin configuration with the payload spinning at a rate of 0.8 Hz (50 rpm) while the bus maintains a stable, nadir-pointing configuration. Mass: 4,5kg
UWE (2005) University of Wrzburg and Fachhochschule Weingarten, Germany.	The attitude of the satellite is passively controlled by means of permanent magnets (in two axis). The axis of no magnet control is selected as the spin axis of the satellite.

Single Momentum Wheel System

Passive three-axis stabilisation of a satellite can be provided by a single momentum wheel with the two axes in the orbit plane being held in their position by the gyroscopic effect of the momentum wheel. Active attitude control about the third axis, which is orthogonal to the orbit plane, is obtained by increasing or decreasing the momentum wheel speed through torquing. A damper must also be included in this system.

Pitch Momentum Wheel/Thruster System

Three-axis active attitude control can be achieved using thrusters for pitch and combined roll/yaw control, and a single momentum wheel mounted along the pitch axis. The wheel spin varies its rate to maintain a constant attitude when a torque acts on the satellite. A momentum unloading system (such as a set of thursters), is needed to desaturate the momentum wheel by reducing its speed to the nominal operating value. As shown in section 2.2.3.

Table 3.2: Small and nanosatellites 3 axis stabilised

ESEO (ESA's Education Satellite Program, University of Bologna, Sitael)	The spacecraft is 3-axis stabilised. The actuator system features 3 redundant orthogonal magnetic coils for attitude acquisition manoeuvres and coarse attitude pointing. An assembly of 4 redundant momentum-biased/reaction wheels is used for fine pointing.
PSSCT-2 (2011) and AeroCube-4 (2012)	It has three reaction wheels supplemented by three magnetorquers for attitude control. The reaction wheels and torque rods were built by the Aerospace Corporation. They demonstrated closed-loop 3-axis attitude control. It had a goal of less than a degree of pointing precision. Aerospace has reported that PSSCT-2 achieved 5 degrees of pointing accuracy and AeroCube-4 demonstrated 3 degrees of pointing accuracy. The reduced accuracy in AeroCube-4 was attributed to the loss of an axis of knowledge of the magnetic field and corruption of the microelectrical mechanical inertial measurement unit (IMU) by helium absorption. Aerospace has planned missions to demonstrate 1 degree and 0.5 degree pointing accuracy on AeroCube-5 and AeroCube-OCSD respectively.
CanX-4 and CanX-5 (2014) (BRITE) University of Toronto	It provides 3-axis stabilisation; the sensors consist of 6 coarse/fine sun sensors, a 3-axis magnetometer, and 3 rate gyros. The combination of these sensor sets yields a pointing accuracy of better than 1. Attitude actuation is provided with 3 orthogonally-mounted reaction wheels (for fine pointing) and 3 magnetorquer coils (for detumbling and momentum dumping). ADCS must be able to slew each satellite such that their propulsion thrusters can deliver the correct impulse in the direction required and with an accuracy of 1. Mass = 15kg
Qb-X1 and Qb-X2 (2010) (Naval Research Laboratory)	These CubeSats, use an International Geomagnetic Reference Field (IGRF) model for rate-damping using magnetorquers. They have a three-reaction wheel and magnetorquer IMI-100 ADCS unit. The controller consists of a combination of passive attitude stabilisation and active rate damping control, using natural gravity gradient torques, aerodynamic drag, and limited use of reaction wheels.

Single-Gimbal Momentum Wheel System

A controller is used to shape the roll error signal and drive the gimbal angle. Rotating the gimbal from null produces a component of angular momentum along the z-axis.

Pitch Momentum Wheel/Yaw Reaction Wheel System

It is an alternative to the single-gimbal momentum wheel system, in which a large momentum wheel is placed along the pitch axis (to provide gyroscopic stiffness) and a small reaction wheel is aligned along the yaw or z-axis. The roll error signal is used to vary the speed of the yaw wheel.

Double-Gimbal Momentum Wheel System

The actuator of this system is a momentum wheel mounted in two-degree-of-freedom gimbals. Except that this system incorporates nutation and orbit rate decoupling, the dynamic behaviour is similar to the one-wheel system with thrusters A signal from a yaw sensor which decouples roll and yaw motion, can also drive this system.

Three Reaction Wheel System

In general, three reaction wheels are required for three axis control, since each produces a torque in a single direction. Considering the most basic form, the system has three reaction wheels aligned along the three principal axis of inertia, to control pitch, yaw and roll.

Reaction wheels control each axis varying the speed in response to the attitude error measured about that axis.The roll and yaw channels are coupled through

vehicle dynamics and there is, consequently, a continuous transfer of momentum between the roll and yaw wheels.

As the wheels absorb disturbance torques, the angular momentum changes slowly with time while the attitude remains fixed. When the wheel reaches saturation, the angular momentum is adjusted by other actuators such as gas jets or magnetorquers. The momentum storage capacity must be sufficient to store both secular and short-duration torques and can be reduced by optimizing the desaturation system. See section 2.2.3.

Advantages of a three-axis stabilised reaction wheel system are:

- Capability of carrying out slew or attitude reorientation manoeuvres about a commanded axis.
- Capability of continuous high-accuracy pointing control.
- Large-angle slewing manoeuvres without fuel consumption.
- Compensation for cyclic torques without fuel consumption.

3.2 Redundancy

For 3-axis control at least three wheels with orthogonal spin axes are required. Often a fourth wheel is carried in case one of the primary wheels fails. If wheels are not orthogonal, additional torque maybe necessary to compensate for non-optimal geometry. Redundancy of the fourth wheel may have additional benefits, such as being able to avoid any wheel speed passing through zero (which can cost attitude

error transients) Or even as power storage, as driving a spinning wheel toward zero speed will provide power to the spacecraft.

Although redundancy guarantee a reduction in mission failures, further strategies shall be considered in case of failure as control laws strategies in case of underactuation. See section 3.3 and Chapter 5.

3.3 Underactuation

There is a heightened interest within several International Space Agencies such as NASA and ESA, for the research of attitude control systems having less than three functional actuators. This interest is raising due to a number of recent wheel failures for some satellite missions and the miniaturization of the AOCS subsystem in nanosatellites which in terms of power and mass could require the use of less than three orthogonal actuators or non redundancies. Some recent mission failures are described in Table 3.3.

The interest in underactuation derives from the need to solve the problem of having a system in which less control variables than the degrees of freedom of the system itself are available. In the case of AOCS of satellites, underactuated control is a scenario where fewer than three actuators are used to provide three axis control.

This condition can be reached due to a failure of any actuator, as explained forehead, or because of an inherent physical property of the system, as for magnetic control. See section 2.2.2.4.

In order to both maintain three-axis attitude control and extend the productivity of the spacecraft that suffer RW in-flight failures [17], different actuator configura-

tions have been proposed as well as improvements on the attitude control algorithms.

An underactuated satellite is a class of a so called non-holonomic system due to the presence of a constraint of this type on the kinematic model. This is when it cannot be integrated to derive a relation between the state variables and the derivatives. When having a non-holonomic constrain, three variables are needed to model the system and the constraint becomes part of the dynamics. [18]. In general, all control laws proposed in the literature for non-holonomic systems are nonlinear singular and time invariant (nonlinear singular) or continuous and time varying (time varying). Conventional smooth control laws cannot stabilise an underactuated satellite modelled as a nonlinear system, therefore, only non-smooth (discontinuous or time varying) control laws can be utilized for the stability of non-holonomic systems. As shown in [19] by Brockett.

Crouch [20], investigated and presented for the first time necessary and sufficient conditions for the controllability of a rigid body in the case of one, two or three independent control torques. He established that, for an arbitrary bias momentum, the stabilisation of the rigid body is impossible (without prior detumbling) using momentum exchange devices (reaction wheels). In the same paper, but in the case of gas jet actuators (thrusters), it was demonstrated that stabilisation is possible for a small time, in the general non-restricted case. This result gave a new interest in underactuated control.

In [21], Byrnes and Isidori excluded the existence of a smooth (static or dynamic) state variable feedback law locally asymptotically stabilising a rigid spacecraft, actuated by three thruster jets, one of which has failed, with two controls. They gave a further result on the instability (in the sense of Lyapunov, see Appendix C) of rigid spacecraft for certain feedback laws, and they were able to construct a feedback

law locally asymptotically driving the closed-loop trajectories to a motion about the third principal axis.

Following these conclusions several researchers came up with different results on how to achieve three-axis stabilisation under certain constrains described in Section 5.1.

Table 3.3: Missions with Wheel failures

Mission	Description
FUSE (1999)	Launched in Circular low Earth orbit (LEO), approximately 725 km in altitude, with an inclination of 25 degrees and with an orbital period around 100 minutes. Zero-momentum, three-axis stabilised spacecraft. FUSE employed a RW-based ACS (four RWs). In November2001, the Yaw RW on FUSE suffered dramatically increased drag and ceased spinning, but science operations continued with the redundant skew RW controlling yaw. In December 2001, the pitch RW also suffered a similar failure. Therefore, 2.5 years after launch, mechanical failures of two out of four RWs reduced the satellite to two-axis control. In July 2007, the skew wheel, failed and efforts to restart it were unsuccessful and the mission was terminated.
TIMED (2001)	Mass: (600kg), Orbit: 625-kilometer circular orbit with an inclination of 74.1 degrees. On 15 February 2007, The RW-1 unit on the TIMED spacecraft exhibited an increase in running friction and it was autonomously removed from the attitude control loop. It was decided to re-design the baseline attitude controller to implement a 2-RW/magnetic torque-rod hybrid control approach.
CASSINI (1997)	A set of four RWs are mounted in the spacecraft. In 20012002, RW-3 exhibited signs of bearing cage instability. Therefore, RW-4 on its platform was aligned with RW-3. Starting in July of 2003 and since then it was controlled using RW-1, RW-2, and RW-4. Cassini is currently using the two remaining functional RWs (i.e., RW-2 and RW-4) and four thrusters for attitude control.

DAWN(2007)	In June 2010 RW-4 was damaged, to preserve the three wheels the backup RCS thrusters were activated for attitude control. An effort was initiated in September 2010 to develop a hybrid control mode that would use only two RWs in a mixed-actuator mode together with thrusters to provide full three-axis attitude control.
Mars Odyssey (2001)	On 8 June 2012, the RW-1 experienced an anomaly. An increase in wheel bearing friction prevented RW-1 from producing the control torque commanded by the AOCS of the spacecraft, which in turn allowed an attitude error. A contingency 2-RW hybrid controller was developed (with thrusters) to maintain three-axis control of the spacecraft in the event of a second wheel anomaly/failure.
KEPLER (2009)	The spacecraft has four RW actuators to generate attitude control torques to slew, point, and precisely stabilise the vehicle. In July 2012, Keplers RW-2 friction increased beyond the control laws torque command; analysis showed friction torque of approximately 140 mN-m, up from a nominal friction torque of 20 mN-m. 2-RW (plus thrusters) hybrid attitude controller for the Kepler spacecraft.
RADARSAT-1 (1995)	Upon the failure of primary and redundant pitch axis wheels, the attitude control system of the satellite was redesigned (and subsequently uploaded while on orbit) to use the remaining wheels and magnetic actuation together. [22].

Chapter 4

CASE 1 - Magnetic and mechanical attitude control strategy for three-axis stabilisation in the orbit frame

4.1 Introduction

This chapter addresses an attitude control strategy for nanosatellites in Low Earth Orbit using both magnetic and mechanical actuation. The system includes three magnetorquers (MTs) and three reaction wheels (RW) as actuators to perform simultaneous attitude control and momentum-management. Control laws drive a rigid nanosatellite towards attitude stabilisation in the orbit frame.

In order to achieve three axis stabilisation, different types of actuators can be selected for AOCS in LEO orbit (See section 2.2.2). While reaction wheels are commonly used to obtain a high precision pointing and fast manoeuvrability, they may suffer from saturation limitations as well as static friction when approaching zero angular velocity. Thus, reaction wheels need a secondary attitude control system

for momentum unloading to desaturate them (Section 2.2.3). In Low Earth orbits (LEO) magnetorquers are a good option for momentum unloading as they provide a cheap, reliable and effective external torque [23]. They can also be a feasible option for attitude control in fully magnetic actuated satellites, or in case of any failure in the main attitude control system.

At least three reaction wheels, or three magnetorquers placed orthogonally, are needed for three-axis control. However, for the case of magnetic control, the inherent underactuation (Section 2.2.2.4) requires specific attitude control strategies for fully magnetic actuation [24, 25] as at any given time instant, the produced torque lies in the orthogonal plane to the instantaneous geomagnetic field leading to the non-controllability of the direction parallel to the local geomagnetic field vector. Until recent years, only approximate solutions to the magnetic attitude control problem were available, [26] and several open issues are related with global formulations.

The torque created due to the interaction of the magnetorquers with the geomagnetic field is not constant. Due to the rotation of the satellite around the Earth, models are almost periodically time-varying. Periodicity assumptions for the magnetic field, have been exploited in the attitude regulation problem [26, 27, 25]. However, time-varying nature of the magnetic field will be considered in this thesis. The time-varying problem has also been recently studied in [28]. In which a B-dot-like control law that detumbles a spacecraft with magnetic actuators is presented. In this case, a rigorous mathematical proof of global asymptotic convergence from arbitrary initial tumbling conditions to zero angular velocity is developed. In this framework, it was proved that in the presence of a time-varying magnetic field, the time derivative of the kinetic energy is strictly decreasing. In [29], with the same assumptions about the magnetic field, a continuous magnetic torque command is proposed, which leads a three-inertial spacecraft to a desired spin condition around

a principal axis of inertia that is aligned towards a target direction, fixed in the inertial reference frame. In [30] a number of different approaches to the above described design problem are compared. In particular, the results obtained using linear time-invariant control laws are compared with the ones provided by periodic optimal state feedback control.

In recent years the use of magnetic and mechanical actuators simultaneously as control strategy has been heightened (See section 3.1). The combined use of the two actuation systems leads to power savings (depending on orbit inclination, control scheme and gains) and less stringent requirements on wheel control torques [31, 22]. Different approaches have been considered throughout the years for AOCS to proof stabilisation respect to different reference frames.

In a recent paper [32], attitude stabilisation with respect to an inertial frame is performed by means of a set of three MWs and three MTs in a similar configuration than the one represented for the case study. In which the mechanical system provided attitude stabilisation and the magnetic torque is only used for momentum dumping of the wheel set. It proposes a new controller which makes the attitude dynamics completely independent of the momentum dumping, as a cascade system, and induces global asymptotic stability of the satellite.

Stabilisation respect to the orbital frame is a being studied to exploit the characteristics of that frame [33]. For certain mission requirements it might be advantageous to stabilise respect to it. (i.e. Pointing an instrument towards a fixed-target direction in the orbit frame). In [33], periodicity assumptions of the magnetic field are considered to stabilise a satellite in the orbit frame, thus this study is a step forward.

This control approach is the extension of a recent result [13] in which the analysis

of simultaneous attitude control and continuous momentum-wheel management of a spacecraft by means of magnetic actuators and one MW is performed. A proof of almost global asymptotic stability is derived for control laws that drive a rigid satellite towards attitude stabilisation. Other recent results on continuous momentum management [34] show the advantage of this technique respect to the periodic one. That result shows a globally stabilising nonlinear feedback control law that enables the tracking of an arbitrary time-varying reference attitude. A redundant cluster of four or more reaction wheels is used to control the spacecraft attitude, and three magnetic torque rods are used for purposes of continuous autonomous momentum dumping.

The continuous momentum dumping strategy using three MTs is considered in this thesis and three-axis stabilisation respect to the orbit frame is demonstrated considering a cluster of three RWs for attitude control. The dynamics of the satellite are represented as a cascade system and the time-varying nature of the magnetic field (not periodicity assumptions) is considered.

The main contribution is the good performance of the control approach which demonstrates continuous momentum management by the magnetorquers and attitude control stabilisation in the orbit frame by the reaction wheels. The theoretical selection of the proper gain and the proof of global asymptotic stability are derived for a satellite pointing an orbital-fixed target direction and robustness to external disturbances and model uncertainties of the proposed control laws are demonstrated by numerical simulations.

4.2 Problem statement and solution

4.2.1 Mathematical Model

For the purpose of this study, spacecraft model in (2.18) can be conveniently reshaped by expressing absolute angular velocity in the form

$$\boldsymbol{\omega} = \boldsymbol{\omega}_{BT} + \boldsymbol{\omega}_{TO} + \boldsymbol{\omega}_{OI} \tag{4.1}$$

where $\boldsymbol{\omega}_{BT}$ is the angular velocity between body and target frame, $\boldsymbol{\omega}_{TO}$ is the angular velocity between target and orbital frame, and $\boldsymbol{\omega}_{OI}$ is the angular velocity between orbital and inertial frame.

Let describe spacecraft attitude with respect to $\mathbb{F}_T$ in terms of quaternion coordinates,

$$\dot{\boldsymbol{q}} = \boldsymbol{W}(q)\,\boldsymbol{\omega}_{BT} \tag{4.2}$$

where $\boldsymbol{q} = (q_1, q_2, q_3, q_4)^T = (\bar{\boldsymbol{q}}^T, q_4)^T$ is the quaternion vector, $\boldsymbol{W}(q) = 1/2\,(q_4\,\mathbb{I}_3 + \bar{\boldsymbol{q}}^{\times} - \bar{\boldsymbol{q}}^T)^T$, and $(\,\cdot\,)^{\times}$ denotes a skew-symmetric matrix. Since $\mathbb{F}_T$ is fixed with respect to $\mathbb{F}_O$, one has $\boldsymbol{\omega}_{TO} = 0$ and $\boldsymbol{\omega}_{OI} = \mathbb{T}_{BT}\,\hat{\boldsymbol{n}}$, provided that

$$\mathbb{T}_{BT} = (\boldsymbol{q}_4^2 - \bar{\boldsymbol{q}}^T\,\bar{\boldsymbol{q}})\mathbb{I}_3 + 2\bar{\boldsymbol{q}}\,\bar{\boldsymbol{q}}^T + 2\bar{\boldsymbol{q}}\,\bar{\boldsymbol{q}}^{\times} \tag{4.3}$$

be the coordinate transformation matrix allowing for vector rotations from $\mathbb{F}_T$ to $\mathbb{F}_B$, and $\boldsymbol{n}$ is the orbital rate. As a result,

$$\boldsymbol{\omega} = \boldsymbol{\omega}_{BT} + \mathbb{T}_{BT}\,\boldsymbol{n} \tag{4.4}$$

and

$$\boldsymbol{I}\dot{\boldsymbol{\omega}} = \boldsymbol{I}\dot{\boldsymbol{\omega}}_{BT} - \boldsymbol{I}\boldsymbol{\omega}_{BT}^{\times}\mathbb{T}_{BT} \tag{4.5}$$

Thus, the dynamics model expressed in Eq. (2.18) becomes

$$\boldsymbol{I}\dot{\boldsymbol{\omega}}_{BT} = \boldsymbol{M} - \dot{\boldsymbol{h}} - (\boldsymbol{\omega}_{BT} + \mathbb{T}_{BT}\,\boldsymbol{n}) \times [\boldsymbol{I}\,(\boldsymbol{\omega}_{BT} + \mathbb{T}_{BT}\,\boldsymbol{n}) + \boldsymbol{h}] + \boldsymbol{I}\boldsymbol{\omega}_{BT}^{\times}\mathbb{T}_{BT}\,\boldsymbol{n} \tag{4.6}$$

4.2.2 Momentum management and attitude stabilisation

Following the concepts introduced in Ref.[13], this section addresses the simultaneous acquisition of an arbitrary attitude in $\mathbb{F}_O$, and satellite angular momentum management by means of magnetic and mechanic actuators. The scope of this section is to prove that the combined use of a time-varying linear control law for the magnetorquers and a quaternion feedback control law for attitude control [35], stabilises spacecraft attitude pointing to a target direction fixed in the orbit frame.

Let $\hat{\boldsymbol{\sigma}} = \mathbb{T}_{BO}\,(0,1,0)^T$ be the unit vector parallel to the direction of the y_O-axis, which is fixed in both the orbit and inertial frames. Two desired angular momentum vectors, $\boldsymbol{H}_d$ and $\boldsymbol{h}_d$, are introduced in the inertial and in the body-fixed frames, respectively. The first vector, defined as $\boldsymbol{H}_d = H_d\,\hat{\boldsymbol{\sigma}}$, where $H_d = ||\boldsymbol{I}\,\boldsymbol{\omega}_d||$ and $\boldsymbol{\omega}_d = \mathbb{T}_{BT}\,\boldsymbol{n}$, implies that the angular momentum is pointing the desired inertially-fixed direction parallel to the orbit normal. The second vector, $\boldsymbol{h}_d = \boldsymbol{0}$, implies the three-axis stabilisation. After defining the angular momentum error variable, $\boldsymbol{\zeta} = \boldsymbol{H}_d - \boldsymbol{h} - \boldsymbol{I}\,\boldsymbol{\omega}$, the model expressed by Eq. (4.6) assumes the form

$$\boldsymbol{I}\dot{\boldsymbol{\omega}}_{BT} = \boldsymbol{M}^{(c)} - \dot{\boldsymbol{h}} - \boldsymbol{\omega}_{BT} \times \boldsymbol{H}_d + \boldsymbol{\omega}_{BT} \times \boldsymbol{\zeta} + \mathbb{T}_{BT}\,\boldsymbol{n} \times \boldsymbol{\zeta} + \boldsymbol{I}\,\boldsymbol{\omega}_{BT} \times \mathbb{T}_{BT}\,\boldsymbol{n} \tag{4.7}$$

provided that $\boldsymbol{M}^{(c)}$ is the magnetic control law

$$\boldsymbol{M}^{(c)} = -k_{\zeta}(\mathbb{I}_3 - \hat{\boldsymbol{b}}\,\hat{\boldsymbol{b}}^T)\boldsymbol{\zeta} \tag{4.8}$$

where $k_\zeta > 0$ is the control gain, $\mathbb{I}_3$ is a 3x3 unit matrix, and $\hat{\boldsymbol{b}} = \boldsymbol{b}/||\boldsymbol{b}||$. Albeit the body axis would be the natural reference system for representing the control moment vector, $\boldsymbol{M}^{(c)}$, the formulation of the magnetic attitude stabilisation problem turns out to be remarkably simple if the attitude dynamics is represented with respect to the inertial frame. Let $\boldsymbol{Z} = \mathbb{T}_{BI}^T \boldsymbol{\zeta}$ be error variable as expressed in the inertial frame, the control moment vector, as well as the error dynamics, is given by

$$\boldsymbol{M}^{(c)} = \dot{\boldsymbol{Z}} = -k_\zeta \left[\mathbb{T}_{BI}^T \left(\mathbb{I}_3 - \hat{\boldsymbol{b}}\, \hat{\boldsymbol{b}}^T \right) \mathbb{T}_{BI} \right] \boldsymbol{Z} \tag{4.9}$$

where $\mathbb{T}_{BI}$ is the coordinate transformation matrix between $\mathbb{F}_I$ and $\mathbb{F}_B$. The control law drives the spacecraft total angular momentum including wheels to a parallel direction to the orbital normal. The controller selected for this attitude control approach is the quaternion feedback control law [35] , which uses the feedback of the unit quaternion and the measured angular velocities to provide global asymptotic stability. The significance of this control law compared with the Euler axis control laws is the performance when large-angle manoeuvres. The aim of the control law is to bring the spacecraft to the desired target attitude starting from any initial attitude.

The time derivative of the total angular momentum of the satellite in the body-fixed, thus $\dot{\boldsymbol{h}}$, is the feedback of quaternion and the angular velocity given by

$$\dot{\boldsymbol{h}} = k_\omega \boldsymbol{\omega}_{BT} + k_q \boldsymbol{q} \tag{4.10}$$

with $k_q > 0$ and $k_\omega > 0$.

4.2.3 Stability analysis

In what follows the proof of asymptotic convergence of proposed control laws is provided.

No external disturbance $\boldsymbol{M}^{(d)}$ is considered in the stability analysis, so that the external torque acting on the spacecraft coincides with the magnetic control torque, namely $\boldsymbol{M}^{(c)} = \boldsymbol{m} \times \boldsymbol{b}$, where $\boldsymbol{m}$ is the magnetic dipole moment vector generated by the MTs and $\boldsymbol{b} = \boldsymbol{T}_{BO}\, \boldsymbol{b}_O$ is the local geomagnetic field vector expressed in terms of body-frame components.

In this proof of closed-loop stability of the control law it will be initially assumed that $\boldsymbol{I} \equiv \boldsymbol{I}^* = \mathrm{diag}(I_1, I_2, I_3)$, that is, $\hat{\boldsymbol{e}}_1$, $\hat{\boldsymbol{e}}_2$, and $\hat{\boldsymbol{e}}_3$ are principal axes of inertia, and $I_2 \neq I_1, I_3$. The presence of off-diagonal terms in $\boldsymbol{I}$ and uncertainties on the elements of $\boldsymbol{I}$ will be dealt within the results section 4.3, in order to assess control law robustness.

By substituting in (4.6) the momentum management and attitude control law, and by rewriting Eq. (2.18), one obtains

$$\begin{aligned}\boldsymbol{I}\dot{\boldsymbol{\omega}}_{BT} = &- k_\zeta \left[\mathbb{T}_{BI}^T \left(\mathbb{I}_3 - \hat{\boldsymbol{b}}\,\hat{\boldsymbol{b}}^T\right) \mathbb{T}_{BI}\right] \boldsymbol{Z} - \boldsymbol{k}_\omega \boldsymbol{\omega}_{BT} - \boldsymbol{k}_q \boldsymbol{q} - \boldsymbol{\omega}_{BT} \times \boldsymbol{H}_d + \\ &+ \boldsymbol{\omega}_{BT} \times \boldsymbol{\zeta} - \boldsymbol{I}^{-1}\boldsymbol{H}_d \times \boldsymbol{\zeta} - \boldsymbol{I}(\boldsymbol{I}^{-1}\boldsymbol{H}_d \times \boldsymbol{\omega}_{BT})\end{aligned} \tag{4.11}$$

$$\dot{\bar{\boldsymbol{q}}} = \frac{1}{2}\left(q_4\, \mathbb{I}_3 + \bar{\boldsymbol{q}}^\times\right) \boldsymbol{\omega}_{BT} \tag{4.12}$$

$$\dot{\boldsymbol{Z}} = -k_\zeta \left[\mathbb{T}_{BI}^T \left(\mathbb{I}_3 - \hat{\boldsymbol{b}}\,\hat{\boldsymbol{b}}^T\right) \mathbb{T}_{BI}\right] \boldsymbol{Z} \tag{4.13}$$

Lemma 4.2.1 *Consider the nonlinear time-varying system defined by Eqs.* (4.11)-(4.13). *The origin* $\left(\boldsymbol{\omega}_{BT}^T, \bar{\boldsymbol{q}}^T,\ \boldsymbol{\zeta}^T \boldsymbol{T}_{IB}\right)^T = \mathbf{0}$ *is globally uniform asymptotically stable (GUAS).*

Proof:.

Considering the Lemma 4.2.1, a stability analysis of the attitude approach is given. Formally, the desirable stabilisation properties for the whole system are presented in a recent result [36], that demonstrates the global uniform stability of cascade non-autonomous non linear time-varying systems.

Let $\boldsymbol{x} = [\boldsymbol{x}_1^T, \boldsymbol{x}_2^T]^T$ be the state variables of the system made of Eqs. (4.11)-(4.13) where $\boldsymbol{x}_1 = \left(\boldsymbol{\omega}_{BT}^T\ \bar{\boldsymbol{q}}^T\right)^T$ and $\boldsymbol{x}_2 = \boldsymbol{T}_{BI}\,\boldsymbol{\zeta}$, matches the standard structure for non linear time varying cascaded systems

$$\begin{cases} \dot{\boldsymbol{x}}_1 = \boldsymbol{f}_1(t, \boldsymbol{x}_1) + \boldsymbol{g}(t, \boldsymbol{x})\boldsymbol{x}_2 \\ \\ \dot{\boldsymbol{x}}_2 = \boldsymbol{f}_2(t, \boldsymbol{x}_2, u) \end{cases} \tag{4.14}$$

where

$$\boldsymbol{f}_1(t, \boldsymbol{x}_1) = \begin{bmatrix} \boldsymbol{I}^{-1}[-\boldsymbol{k}_\omega \mathbb{I}_3 + \boldsymbol{H}_d^x - I[(\boldsymbol{I}^{-1}\boldsymbol{H}_d)^x] & -\boldsymbol{I}^{-1}\boldsymbol{k}_q \\ 1/2(\boldsymbol{q}_4 + \boldsymbol{q}_r^x) & 0 \end{bmatrix} \begin{bmatrix} \boldsymbol{\omega}_{BT} \\ \boldsymbol{q} \end{bmatrix} \tag{4.15}$$

and

$$\boldsymbol{g}(t, \boldsymbol{x}) = \boldsymbol{I}^{-1}\left[-k_\zeta\, \mathbb{T}_{BI}^T \left(\mathbb{I}_3 - \hat{\boldsymbol{b}}\,\hat{\boldsymbol{b}}^T\right) \mathbb{T}_{BI} + \boldsymbol{\omega}_{BT}^\times + \boldsymbol{I}^{-1}\boldsymbol{H}_d^\times\right] \tag{4.16}$$

Being $\boldsymbol{f}_1(t, \boldsymbol{x}_1)$ continuously differentiable in $(t, \boldsymbol{x}_1)$ and as $\boldsymbol{g}(t, \boldsymbol{x})$ continuous in its arguments. Sufficient conditions are given to guarantee that if $\boldsymbol{f}_1(t, \boldsymbol{x}_1)$ is GUAS and $\dot{\boldsymbol{x}}_2 = \boldsymbol{f}_2(t, \boldsymbol{x}_2, u)$ is GES then the cascade is GUAS

Globally uniform stability of the cascade system is provided by Theorem 1 in [36], if the A1-A3 assumptions are satisfied.

Assumption 1 *: The system* $\dot{\boldsymbol{x}}_1 = \boldsymbol{f}_1(t, \boldsymbol{x}_1)$ *is globally uniformly stable with a positive definite and proper Lyapunov function* $\boldsymbol{V}(t, \boldsymbol{x}_1)$*.*

Let

$$\boldsymbol{V} = \frac{1}{2}\,\boldsymbol{\omega}_{BT}\boldsymbol{I}\boldsymbol{\omega}_{BT} + k_q\left[\boldsymbol{q}^T\boldsymbol{q} + (\boldsymbol{q}_4 - 1)^2\right] \tag{4.17}$$

be a Lyapunov candidate. Its time derivative is

$$\begin{aligned}\dot{\boldsymbol{V}} =& \boldsymbol{\omega}_{BT}^T\left[\boldsymbol{k}_\omega - \boldsymbol{I}[(\boldsymbol{I}^{-1}\boldsymbol{H}_d)^x]\right]\omega_{BT} + \boldsymbol{\omega}_{BT}^T[-\left(\mathbb{I}_3 - \hat{\boldsymbol{b}}\,\hat{\boldsymbol{b}}^T\right)(k_\zeta) + \\ &+ (\boldsymbol{I}^{-1}\boldsymbol{H}_d)^x]\boldsymbol{\zeta} + \boldsymbol{k}_q\boldsymbol{q}\boldsymbol{\omega}_{BT}^T - \boldsymbol{k}_q\boldsymbol{q}\boldsymbol{\omega}_{BT}^T\end{aligned} \tag{4.18}$$

and being $[-\boldsymbol{I}[(\boldsymbol{I}^{-1}\boldsymbol{H}_d)^x]$ a skew-symmetric matrix, the Lyapunov candidate satisfies the conditions 1-3 of Corollary 1, see Appendix A, to guarantee that Eq. (4.17) is a proper function of the proposed system.

Assumption 2 *: The input vector* $\boldsymbol{g}(\boldsymbol{t}, \boldsymbol{x})$

$$\|\boldsymbol{g}(\boldsymbol{t}, \boldsymbol{x})\| <= \|\theta_1(\|\zeta\|)\| + \|\theta_2(\|\zeta\|)\|\|\boldsymbol{x}_1\| \tag{4.19}$$

Assumption 3 *: The control law* (4.13) *is globally exponentially stable, uniformly in t (GES).*

Stability proof of the control law in Eq. (4.9) was demonstrated in a recent paper [37], and it is included in Appendix A.

Considering the Theorem 2 in [36], under the assumptions A1-A3, of theorem 1; assuming additionally that the system $\boldsymbol{f}_1(t, \boldsymbol{x}_1)$ is globally asymptotically stable uniformly in t (GUAS), and having demonstrated that $\dot{\boldsymbol{x}}_2$ is GES [36], it can be concluded the cascaded system, Eq. (4.14) is GUAS.

4.2.4 Choice of the control gain

A reasonable choice for the control gain, k_ζ , that allows for reaching the desired spinning condition in quasi–minimum time, can be derived by following an approach similar to that derived in Ref.[28] for the detumbling manoeuvre. A few differences need to be taken into account:

1. The whole system is represented in terms of angular momentum dynamics.
2. A value of the desired final angular rate $\bar{\omega}_{BT} = 0$ is expected at the end of the manoeuvre, which in turn requires the following.
3. The whole procedure is rephrased in terms of closed loop dynamics of the component of the error $\boldsymbol{Z}$ perpendicular to the Earth's magnetic field, defined as $\boldsymbol{Z}_\perp = -k_\zeta \, (\mathbb{I}_3 - \hat{\boldsymbol{b}}\,\hat{\boldsymbol{b}}^T)\,\boldsymbol{Z}$. The magnetic field is expressed in terms of inertial frame. The gain is then sized assuming that the error signal is a first order perturbation of the desired final condition.

The time derivative of $\boldsymbol{Z}_\perp$ is given by

$$\begin{aligned}\frac{d\boldsymbol{Z}_\perp}{dt} &= (\mathbb{I}_3 - \hat{\boldsymbol{b}}\,\hat{\boldsymbol{b}}^T)\,[-k_\zeta\,(\mathbb{I}_3 - \hat{\boldsymbol{b}}\,\hat{\boldsymbol{b}}^T)\,\boldsymbol{Z}] \\ &\quad - \left[\frac{d\,\hat{\boldsymbol{b}}}{dt}\,\hat{\boldsymbol{b}}^T + \hat{\boldsymbol{b}}\left(\frac{d\,\hat{\boldsymbol{b}}}{dt}\right)^T\right]\boldsymbol{Z}\end{aligned} \tag{4.20}$$

$$\left[\frac{d\,\hat{\boldsymbol{b}}\boldsymbol{b}}{dt}\,\hat{\boldsymbol{b}}^T + \hat{\boldsymbol{b}}\left(\frac{d\,\hat{\boldsymbol{b}}}{dt}\right)^T\right] = \mathbb{T}_{IO}\left[\frac{d\,\hat{\boldsymbol{b}}_o}{dt}\,\hat{\boldsymbol{b}}_o^T + \hat{\boldsymbol{b}}_o\left(\frac{d\,\hat{\boldsymbol{b}}_o}{dt}\right)^T\right]\mathbb{T}_{IO}^T \tag{4.21}$$

$$-\tilde{\Omega_{IO}}(\hat{\boldsymbol{b}}\boldsymbol{b}) + (\hat{\boldsymbol{b}}\boldsymbol{b})\tilde{\Omega_{IO}} = \mathbb{T}_{IO}^T\mathcal{B}\mathbb{T}_{IO} - \mathcal{C}$$

Equation (4.20) can thus be recast in the form

$$\frac{d\boldsymbol{Z}_{\perp}}{dt} \cong -k_{\zeta}\, \mathcal{A}\, \boldsymbol{Z} - \mathbb{T}_{IO}\, \mathcal{B}\, \mathbb{T}_{IO}^{T}\, \boldsymbol{Z} + \mathcal{C}\, \boldsymbol{Z} \tag{4.22}$$

where $\mathcal{A} = (\mathbb{I}_3 - \hat{\boldsymbol{b}}\hat{\boldsymbol{b}}^T)$ is the projection operator, and the last two terms, namely

$$\mathcal{B} = (1/\|\boldsymbol{b}_O\|^2) \left[\dot{\boldsymbol{b}}_O \boldsymbol{b}_O^T + \boldsymbol{b}_O \dot{\boldsymbol{b}}_O^T - \frac{2}{\|\boldsymbol{b}_O\|^2} (\dot{\boldsymbol{b}}_O^T \boldsymbol{b}_O) \boldsymbol{b}_O \boldsymbol{b}_O^T \right] \tag{4.23}$$

and

$$\mathcal{C} = \tilde{\boldsymbol{\Omega}}_{IO}(\hat{\boldsymbol{b}}\hat{\boldsymbol{b}}^T) - (\hat{\boldsymbol{b}}\hat{\boldsymbol{b}}^T)\tilde{\boldsymbol{\Omega}}_{IO} \tag{4.24}$$

are related to the rotation rate of the Earth magnetic field vector with respect to $\mathbb{F}_I$. Only the first term in Eq. (4.22) (named the active term) is directly related to the control torque and it affects the magnitude of $\boldsymbol{Z}_{\perp}$, whereas the other terms, the gyroscopic and the rotational terms, only affect the direction of $\boldsymbol{Z}_{\perp}$ in the body frame. $\boldsymbol{Z}$

As explained in more detail in Ref. [28], high values of k_{ζ} cause the magnitude of the transverse component $\boldsymbol{Z}_{\perp}$ to rapidly vanish and, as a consequence, also the available control moment becomes small. The only possibility to further decrease $\|\boldsymbol{Z}\|$ relies on the residual angle between $\boldsymbol{b}$ and $\boldsymbol{Z}$ induced by the (slow) rotation of $\boldsymbol{b}$ with respect to the orbit frame, $\mathbb{F}_O$, which allows for a residual controllability. Moreover, a small value of the gain causes a slow closed–loop dynamics, with long convergence time before the desired attitude is reached.

A compromise can be obtained by imposing that the order of magnitude of the active term is equivalent to that of the rotational and gyroscopic ones in Eq. (4.22):

$$\mathcal{O}\left(\|k_{\zeta}\, \mathcal{A}\, \boldsymbol{Z}\|\right) = \mathcal{O}\left(\|\mathbb{T}_{IO}\, \mathcal{B}\, \mathbb{T}_{IO}^{T}\, \boldsymbol{Z} - \mathcal{C}\, \boldsymbol{Z}\|\right) \leq \mathcal{O}\left(\|\mathcal{B}\boldsymbol{Z}\|\right) + \mathcal{O}\left(\|\mathcal{C}\, \boldsymbol{Z}\|\right) \tag{4.25}$$

The order of the active term, $\mathcal{A}\, \boldsymbol{Z}$, and of the first rotational term, $\mathcal{B}\, \boldsymbol{Z}$, can be derived from the discussion presented in Ref.[28]. Given the definition of norm

for a linear operator, $\|\boldsymbol{M}\| = \max_{\boldsymbol{v}\in\mathbb{R}^n}(\|\boldsymbol{M}\boldsymbol{v}\|/\|\boldsymbol{v}\|) = \max_{1\leq i\leq n}(|\lambda_i^{\boldsymbol{M}}|)$, where $\lambda_i^{\boldsymbol{M}}$, $i = 1, 2, \ldots, n$ are the eigenvalues of $\boldsymbol{M}$, one gets that $\|\mathcal{A}\,\boldsymbol{Z}\| = \mathcal{O}(\boldsymbol{Z})$ and $\|\mathcal{B}\,\boldsymbol{Z}\| = \mathcal{O}(2\,\Omega\,\sin\,\xi_m)$.

The procedure described for the determination of $\mathcal{O}(\|\mathcal{C}\,\boldsymbol{Z}\|)$ can be adopted here. This means that $\|\mathcal{C}\,\boldsymbol{Z}\| = \mathcal{O}(2\Omega)$ Provided that $\Omega \ll \bar{\omega}_d$, the third term in Eq. (4.20) is negligible and it can be dropped.

The remaining ones are required to satisfy

$$k_\zeta max\mathcal{A} = max\mathcal{B} + max\mathcal{C} \tag{4.26}$$

$$k_\zeta = 2\,\Omega\,(1 + \sin\,\xi_m) \tag{4.27}$$

This criterion provides an upper bound for the control gain, where higher values are expected to cancel the component of $\boldsymbol{Z}$ perpendicular to $\hat{\boldsymbol{b}}$ too soon.

4.3 Simulation Results

A series of Montecarlo simulations have been performed in order to assess robustness of the control strategy proposed. A non-linear model for spacecraft attitude dynamics has been considered for the simulations (Eq.(2.18)) .

In table 4.2 the initial conditions and gains used for a sample maneuver are shown. Whilst table 4.1 shows relevant spacecraft data, orbit and environmental parameters applied to a LEO microsatellite [38] [1] equipped with three mutually

[1]This is the case of European Student Earth Orbiter (ESEO), a LEO microsatellite mission that is being developed, integrated, and tested by European university students as an ESA Education Office project. In this platform, three-axis pointing with respect to the orbit frame is required for Earth observation and the attitude control system is equipped with a set of magnetorquers and an assembly of 4 redundant momentum-biased/reaction wheels is used for fine pointing.

orthogonal magnetorquers, in the case of having three reaction wheels such that, no friction is considered for the wheel assembly.

The three most relevant sources of external disturbance torque in LEO are included in the model used for the simulations discussed, namely gravity gradient, aerodynamic, solar radiation pressure and residual magnetic torques. Environmental disturbances are applied to the spacecraft model and off-diagonal terms are present in the spacecraft inertia matrix. To demonstrate robustness in the presence of these terms, the spacecraft principal axes are offset from the spacecraft body axes by considering the matrix $\tilde{\boldsymbol{I}} \neq \boldsymbol{I}$. See table 4.1.

The initial phase in which the satellite is magnetically detumbled after orbit injection is not analized in this thesis as not relevant to the aim of the present study and let assume that after the initial detumbling phase [39, 28], the spacecraft lies in a random attitude initial condition (see Table 4.2). During the maneuver it is expected that angular momentum is dissipated by MTs.

The gain for the magnetic control law is $k_\zeta = 0.004$ it is the upper bounded value of the gain described in 4.2.4, whereas the gains for the quaternion control law of the wheel are $k_\omega = 0.1$ and $k_q = 0.008$. The motivation of the choice of the control gains for the quaternion feedback control law is described in Appendix B.

Time histories of angular momenta of the wheels are reported in Fig. 4.1, as well as the spacecraft angular momentum error approaching to zero. Attitude expressed in quaternion is shown in Fig. 4.2 and the quaternion error is also converging to zero.

Figure 4.3 shows that the MTs initially saturate when the errors are large. At the same time, quaternion feedback control law distributes the angular momentum

between spacecraft and RWs, driving the body frame to three-axis stabilisation with respect to the orbit frame in less than 0.07 orbit.

In order to see the performance in a more real scenario, white noise is added to each Euler angle and angular velocity measurement, with standard deviation 1.07 deg and 0.01 deg/s, respectively, to simulating the effects of sensor noise.

In steady state conditions, the error variables remain bounded in the presence of disturbances. Quaternion and spacecraft angular rates with respect to the target frame oscillate with a pointing accuracy of 0.002 and 0.006 deg/s, on each axis in terms of standard deviation. Statistical analysis is performed over 10 orbits in steady-state conditions.

The control law simulations demonstrate the feasibility of the proposed approach and, in particular, illustrate the ability of the controllers to drive the spacecraft to attitude stabilisation as it was derived in the stability analysis.

Robustness of the closed loop system is also shown with respect to external disturbance torque, measurement noise, and model uncertainty.

The control law approach simulations perform well and attitude control and continuous momentum management are achieved for the cascade system which is stabilised in orbit frame.

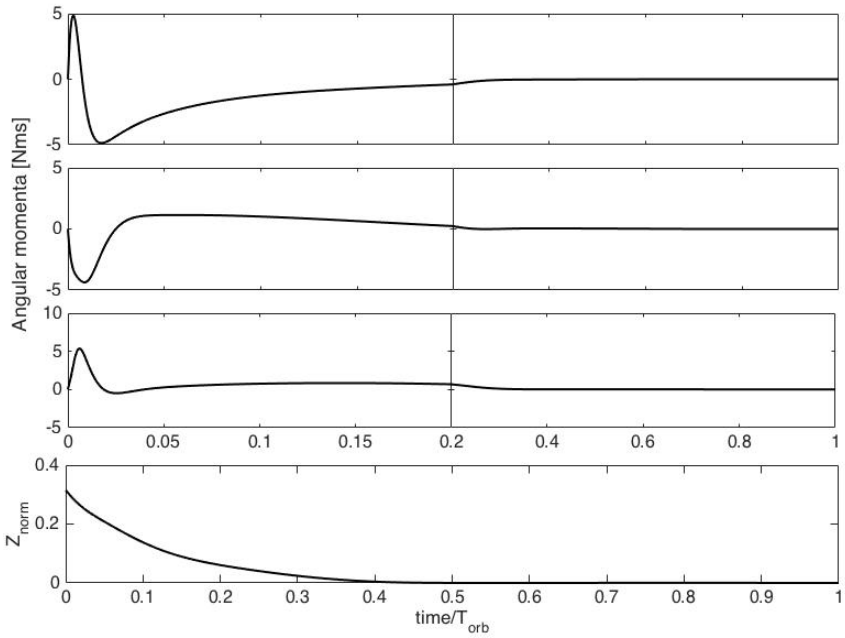

Figure 4.1: Wheel angular momenta and spacecraft momentum error

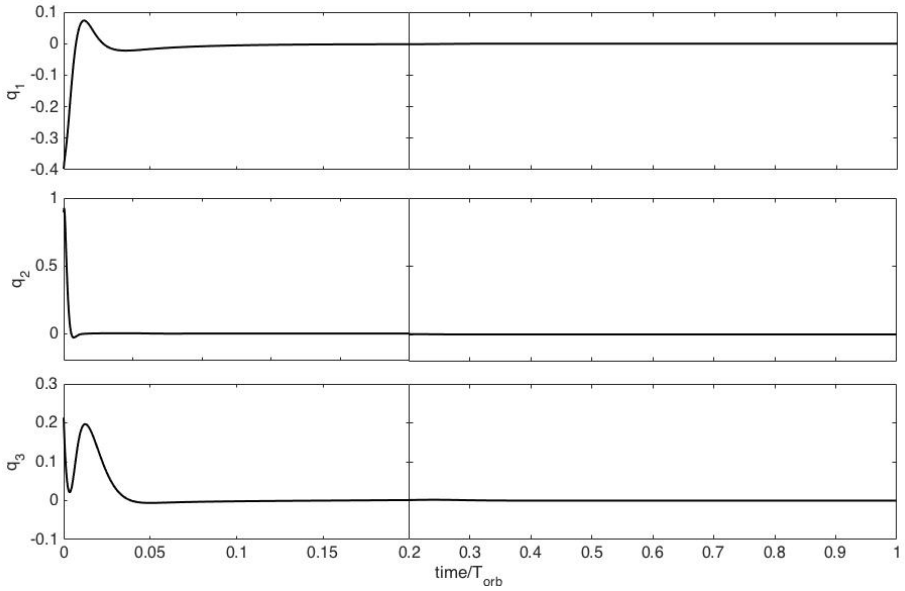

Figure 4.2: Spacecraft attitude quaternions

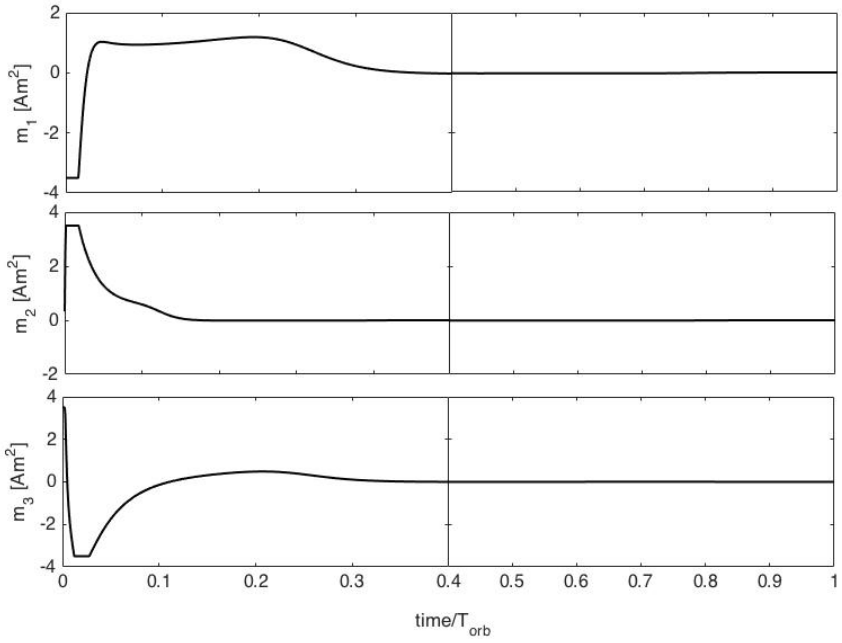

Figure 4.3: Magnetorquers efforts

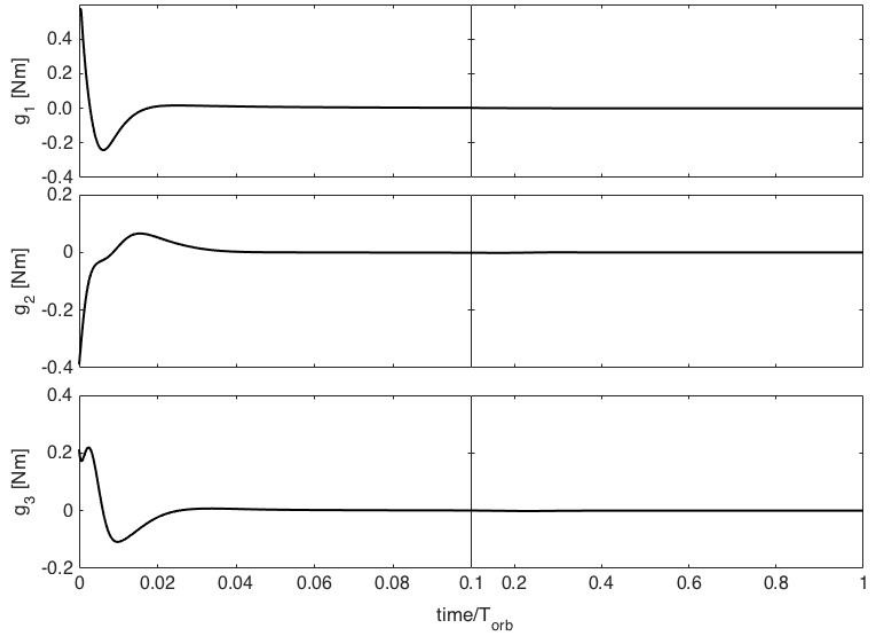

Figure 4.4: Wheel efforts

Table 4.1: Spacecraft, orbit and environment data

Parameter	Symbol	Value	Units
Spacecraft data			
Principal moments of inertia	$J_1,\ J_2,\ J_3$	2.023, 2.060, 0.865	kg m^2
Inertia matrix with offset	$J_1,\ J_2,\ J_3$	1.9384, 2.0861, 0.8939	kg m^2
	$J_{12} = J_{21}$	0.0134	kg m^2
	$J_{23} = J_{32}$	-0.0286	kg m^2
	$J_{31} = J_{13}$	-0.0016	kg m^2
Wheels moment of inertia	J_w	4.20×10^{-4}	kg m^2
Maximum magnetic dipole(per axis)	$m_{\max}$	3.5	A m^2
Maximum wheel torque(per axis)	$g_{\max}$	0.01	N m
Dimensions	$l_1,\ l_2,\ l_3$	0.3, 0.6, 0.3	m
Environment data			
Drag coefficient	C_D	2.2	
Air density	ρ	$6.39 \cdot 10^{-13}$	kg/m^3
Residual magnetic dipole	$\boldsymbol{m}_{rm}$	$(0.1, 0.1, 0.1)^T$	Am^2
Orbit data			
Radius	r_c	6 905	km
Period	T_{orb}	5710	s
Inclination	i	98	deg

Table 4.2: Gains and initial conditions for a sample manoeuvre.

Parameter	Symbol	Value
Gains		
Magnetic Control Law	k_ζ	0.004
Quaternion feedback	k_ω	0.1
	k_q	0.008
Sample manoeuvre		
Initial Conditions	$\boldsymbol{\omega}_T 0$	$(0,\ 0.0297,\ 0)^T$ rad/s
	$\boldsymbol{Q}_T 0$	$(-0.38,\ 0.88,\ 0.21,\ 0.037)^T$

Chapter 5

CASE 2 - Slew manoeuvre and three-axis attitude stabilisation of an underactuated nanosatellite

5.1 Introduction

The aim of the research described in this chapter is to develop a stable control methodology for three axis stabilisation of a spacecraft in underactuated conditions due to a failure of a reaction wheel. The control scheme will consist of a dynamical implementation of an attitude manoeuvre planning by means of a sequence of 2 admissible rotations, where a rotation is considered to be admissible if it takes place around an axis which lies on the plane where the actuator system can deliver a control torque with the aim of driving an underactuated satellite towards a desired target attitude. Simulations will be performed to validate the control scheme and a proof of asymptotic stability will be described forward.

The problem of the underactuation described in Section 3.3 covers a very broad spectrum. Different solutions to deal with the scenario where fewer than three actu-

ators for three axis attitude control have been proposed over the last two decades. A preventive solution to deal with this particular scenario is to include redundant actuators in the satellite. However, the increase in the mass of the satellite might not be a feasible solution and the enhancements in attitude control algorithms may represent the most cost-effective solution to improve the overall system quality. [40].

Although recent studies show a limited need for the development of new, or improvement of existing, analytical (modelling and simulation) tools for ACS, the performance of large-angle spacecraft attitude slew manoeuvres (for communications or power purposes) continues to be a common stressing challenge for 2-RW attitude control [17].

In this framework, different strategies have been applied for the detumbling problem [41, 19, 42], attitude stabilisation [43, 44, 45, 46, 47, 48, 49] and attitude tracking or manoeuvring [41, 50, 51, 52, 53, 54] of a spacecraft.

The problem of three axis stabilisation with actuated angular velocities as virtual inputs for $\omega_3(0) = 0$ was studied by [43, 55]. Morin proposed a continuous time-varying feedback control law for asymptotic stabilisation while Kim proposed a set of control laws including kinematics and dynamics and achieving global asymptotic stabilisation for the closed-loop nonlinear system.

Concerning the underactuated attitude control using two reaction wheels, Krishnan [48, 56] proposed a control strategy to stabilise a rigid satellite using two momentum wheels under the restriction of zero-momentum, which means that the total angular momentum of the whole system is zero. He showed that if the uncontrolled principal axis is not an axis of symmetry, then the complete dynamics are small time locally controllable. However, the satellite cannot be asymptotic stabilised

to any equilibrium attitude using smooth feedback and discontinuous feedback was constructed to accomplish a sequence of manoeuvres.

A new parametrisation technique was used by Tsiotras in [57] who proposed an approach to deal with the stabilisation problem with two pairs of thrusters for axis-symmetrical underactuated spacecraft. More details are further published in [58]. He proposed a time-invariant feedback control law to asymptotically stabilise and control attitude. He also developed reduced effort control laws [59], optimal and time optimal [60, 61]and with bounded inputs in [41]and a survey of all of these techniques was shown in [41]

Different control techniques have been developed and applied for the underactuation problem. Continuous feedbacks which are functions of the state only, cannot locally asymptotically stabilise rigid body models with two controls. If the feedback is also a function of time, this impossibility no longer holds and time-varying asymptotically stabilising feedbacks have been proposed. In [43], exponential convergence is obtained by considering time-varying feedbacks which are only continuous. In [45], Han et al. developed time-varying nonlinear controllers for underactuated attitude control with two reaction wheels. Seol et al. [62] proposed a momentum transfer control of a rigid spacecraft with two momentum wheel actuators using the feedback linearisation technique in which the equations of motion are transformed to a general linearised form and a guarantee of internal dynamics stability is shown. Open-loop control laws have been designed for a two-wheeled satellite. In [63] Alamir deals with the open-loop attitude control of a satellite actuated by two reaction wheels when the kinetic momentum is not necessarily equal to zero and Ge [64] transforms the problem of reorientation into an optimal control problem considering a genetic algorithm to derive the control laws of the two flywheels angle velocity inputs and demonstrating that is an effective approach. Hall [65] proposed a

time-invariant, piecewise-smooth quaternion feedback regulator based on generalised inverse method to affect three-axis stabilisation of the error quaternion kinematics of an underactuated rigid satellite with arbitrary matrix and two bounded body-fixed torques. In [66] stability by smooth feedback of the angular velocity of a rigid body is discussed showing how to asymptotically stabilise the system with a single control. Then it is shown that a single control aligned with a principal axis cannot asymptotically stabilise the system and some results on stabilisation by means of scalar feedback control are presented.

Research on underactuated attitude control indicates that model uncertainties and disturbances, especially those applied on the underactuated axis, greatly influence the accuracy of underactuated attitude control and in general, the stability.

In [47, 67], the angular momentum of the system is not zero but small and the behaviour of the controlled system is investigated. When this happens, the system converges to either a limit cycle or an equilibrium point which is not the desired point; however, in both cases, the error in attitude remains small. Horri and Hodgart [47] proposed a time-invariant control law for the stabilisation and control of attitude and attitude rate of a nearly symmetric rigid satellite using two momentum wheels.

Some control approaches show robustness to disturbances. This is the case of Han and Pechev [44], they derived a control law and a set of control gains that guarantee stability and disturbance attenuation properties through a dissipation analysis. Three axis attitude stabilisation and control is delivered using only two control inputs supplied by two parallel CMGs. More recently, in [68] they proposed an approach using the principle of non-linear $H\infty$ design to improve the pointing accuracy and robustness of one popular underactuated attitude control design, which was presented by Tsiotras et al. stabilising the underactuated attitude system.

In this thesis the tracking of the angular velocity will be considered. A similar strategy is shown in [18], in which the three axis attitude control problem with just two reaction wheels is addressed, and two approaches are proposed and compared. One does not require angular velocity measurements and is based on the assumption of a perfect zero momentum, while the second approach consists of tracking the desired angular velocity trajectories. The full-state feedback is a nonlinear singular controller and inverse optimization theory is applied to enhance the nonlinear singular controller showing more efficiency. The resulting switched inverse optimal controller allows for a significant enhancement of settling time, for a prescribed level of the integrated torque.

The new control approach developed in this thesis has interesting similarities with of the one proposed in [47] by Horri et al. who showed that attitude is precisely and rapidly restored, without transient oscillations, using a nonlinear time invariant and discontinuous control law, combined with the idea of using a sequence of two rotations [69] to achieve the desired attitude by means of a switching control law.

5.2 Problem statement and methods

In this section, the switching control law will be described in detail. Firstly the two-step kinematic manoeuvre is presented followed by the mathematical model of the underactuated satellite. The control approach will be described further as well as the stability proof and the results obtained in the validation process through numerical simulations.

5.2.1 Overview of the two-step kinematic steering technique for attitude acquisition

A detailed description of a set of kinematic planning techniques for slew manoeuvres of underactuated spacecraft based on a sequence of N admissible rotations is presented in Reference [69].

An admissible rotation is a rotation that take place around an axis $\hat{\boldsymbol{g}}$ which lies on the plane perpendicular to the underactuated or torqueless direction $\hat{\boldsymbol{b}}$. The problem cannot be solved for $N = 1$, but it admits an exact solution for $N = 2$. In this case, it is possible to select for the first rotation an arbitrary axis $\hat{\boldsymbol{g}}_1$ on the plane $\Gamma \perp \hat{\boldsymbol{b}}$.

The first rotation angle $\hat{\phi}_1$ is identified by enforcing the condition that the vector part $\boldsymbol{\epsilon}$ of the quaternion error $\boldsymbol{E} = (\boldsymbol{\epsilon}^T, \epsilon_4)^T$ after the first rotation becomes perpendicular to $\hat{\boldsymbol{b}}$. The direction $\hat{\boldsymbol{g}}_2 = \boldsymbol{\epsilon}/\|\boldsymbol{\epsilon}\|$ is selected as the axis for the second admissible rotation, the amplitude of which is simply given by $\hat{\phi}_2 = \cos^{-1}(\epsilon_4)$. A solution for minimum angular travel $\hat{\phi}_1 + \hat{\phi}_2$ can be analytically identified. For $N > 2$ a numerical optimisation technique needs to be adopted.

It is assumed that the initial attitude $\mathcal{F}_{B_0}$ coincides with the fixed frame, $\mathcal{F}_I$, where $\hat{\boldsymbol{e}}_3 = \hat{\boldsymbol{b}}$ is the torqueless direction. The desired attitude is represented by the quaternion $\boldsymbol{P} = (\boldsymbol{p}^T, p_4)^T$, where $\boldsymbol{p} = (p_1, p_2, p_3)^T = \hat{\boldsymbol{e}} \sin(\phi/2)$ and $p_4 = \cos(\phi/2)$, which is associated to the nominal Euler eigenaxis rotation ϕ around the eigenaxis $\hat{\boldsymbol{e}}$, which rotates $\mathcal{F}_{B_0}$ onto the target attitude, identified by the reference frame, $\mathcal{F}_T$.

Letting λ be the angle between $\hat{\boldsymbol{b}} \equiv \hat{\boldsymbol{e}}_3 = (0, 0, 1)$ and the nominal eigenaxis $\hat{\boldsymbol{e}}$, it is possible to choose without loss of generality the first axis of the body frame, $\hat{\boldsymbol{e}}_1$ along the direction of the projection of $\hat{\boldsymbol{e}}$ on the plane Γ, with $\hat{\boldsymbol{e}}_2$ completing a right-

handed frame. In this way, the nominal eigenaxis is given by $\hat{\boldsymbol{e}} = (\sin\lambda, 0, \cos\lambda)^T$ and the target attitude is described by the quaternion

$$\boldsymbol{P} = (\sin\lambda\sin(\phi/2), 0, \cos\lambda\sin(\phi/2), \cos(\phi/2))^T$$

The attitude after the first rotation $\hat{\phi}_1$ around $\hat{\boldsymbol{g}}_1$ is associated to the quaternion $\boldsymbol{Q} = (\boldsymbol{q}^T, q_4)^T$, with $\boldsymbol{q} = (q_1, q_2, q_3)^T = \hat{\boldsymbol{g}}_1 \sin(\hat{\phi}_1/2)$ and $q_4 = \cos(\hat{\phi}_1/2)$, where $\hat{\boldsymbol{g}}_1 = (\cos\alpha, \sin\alpha, 0)^T$, provided α is the angle between $\hat{\boldsymbol{g}}_1$ and $\hat{\boldsymbol{e}}_1$. Thus, $\boldsymbol{Q} = (\cos\alpha\sin(\hat{\phi}_1/2), \sin\alpha\sin(\hat{\phi}_1/2), 0, \cos(\hat{\phi}_1/2))^T$.

Denoting with $\boldsymbol{Q}^\star = (-\boldsymbol{q}^T, q_4)^T$ the conjugate quaternion, such that $\boldsymbol{Q}\boldsymbol{Q}^\star = \boldsymbol{Q}^\star\boldsymbol{Q} = (0,0,0,1)^T$, the quaternion error vector $\boldsymbol{E} = \boldsymbol{Q}^\star\boldsymbol{P}$ can be obtained by application of the quaternion multiplication rule, where

$$\boldsymbol{\epsilon} = q_4\boldsymbol{p} - p_4\boldsymbol{q} - \boldsymbol{q}\times\boldsymbol{p}\ , \quad \epsilon_4 = q_4 p_4 + \boldsymbol{q}^T\boldsymbol{p} \tag{5.1}$$

The condition $\hat{\boldsymbol{b}}^T\boldsymbol{\epsilon} = 0$ is enforced by choosing $\hat{\phi}_1$ such that

$$\cos(\hat{\phi}_1/2)\cos\lambda + \sin\lambda\sin\alpha_1\sin(\hat{\phi}_1/2) = 0 \tag{5.2}$$

that is

$$\tan(\hat{\phi}_1/2) = -\cos\lambda/(\sin\alpha_1\sin\lambda) \tag{5.3}$$

In the present application, rather than pursuing the solution minimising the total angular travel $\hat{\phi}_1 + \hat{\phi}_2$ derived in [69], one can note that for $\alpha_1 = \pi/2$ the angle $\hat{\phi}_1$ is minimised, that is, the amplitude of the rotation that drives the Euler eigenaxis onto the plane of admissible rotations. In this case, the direction of $\hat{\boldsymbol{g}}_1$ is perpendicular to both $\hat{\boldsymbol{e}}$ and $\hat{\boldsymbol{b}}$ unit vectors, that is, it can be easily expressed in the form

$$\hat{\boldsymbol{g}}_1 = (\hat{\boldsymbol{b}}\times\hat{\boldsymbol{e}})/\|\hat{\boldsymbol{b}}\times\hat{\boldsymbol{e}}\| \tag{5.4}$$

without the need for any trigonometric calculation.

5.2.2 Mathematical model of the underactuated satellite - kinematics and dynamics

A satellite platform equipped with three identical reaction wheels is considered. In the case of a failure of the yaw-wheel, just two control torques are available and the spacecraft become underactuaded (See section 3.3).

In general, spacecraft dynamics is described by the following equation of motion

$$\boldsymbol{I}\,\dot{\boldsymbol{\omega}} + \dot{\boldsymbol{h}} + \boldsymbol{\omega} \times (\boldsymbol{I}\,\boldsymbol{\omega} + \boldsymbol{h}) = \boldsymbol{M}$$

it is Eq.(2.18) presented in Section 2.2 where $\boldsymbol{\omega} = (\omega_1, \omega_2, \omega_3)^T$ is the absolute angular velocity vector with respect $\mathbb{F}_I$, $\boldsymbol{I}$ is the spacecraft inertia matrix, $\boldsymbol{h} = (h_1, h_2, h_3)^T$ is the angular momentum vector, and $\boldsymbol{M} = (M_1, M_2, M_3)^T$ is the external torque vector.

As a result, in the absence of external disturbance torques, the dynamics equation reduces to

$$\boldsymbol{I}\dot{\boldsymbol{\omega}} = -\boldsymbol{\omega} \times (\boldsymbol{I}\boldsymbol{\omega} + \boldsymbol{h}) + \boldsymbol{u} \tag{5.5}$$

where the control torque is $\boldsymbol{u} = -\dot{\boldsymbol{h}}$. Which can also be expressed as

$$\dot{h}_{w,i} \;=\; I_w\dot{\Omega}_i \;=\; g_i - I_w\dot{\boldsymbol{\omega}}^T\hat{\boldsymbol{a}}_i, \quad i = 1, 2, 3 \tag{5.6}$$

The quantity $h_{w,i} = J_w\Omega_i$ represents the relative angular momentum vector of the i-th reaction wheel, spinning at a relative angular rate Ω_i around the control axis $\hat{\boldsymbol{a}}_i$, under the action of an electrical motor torque g_i, and $\boldsymbol{J}$ is the satellite inertia matrix. The vector $\boldsymbol{h}_w = \sum_{i=1}^{3} J_w\Omega_i\hat{\boldsymbol{a}}_i$ is the total internal angular momentum. It is assumed that principal axes of inertia are parallel to wheel spin axes, $\hat{\boldsymbol{e}}_i = \hat{\boldsymbol{a}}_i$, $i = 1, 2, 3$.

Without loss of generality, it is assumed that an actuator has failed on the Z axis $h_3 = 0$,the underactuated axis is $\hat{\boldsymbol{b}} = \hat{\boldsymbol{e}}_3$. As a consequence, only two RW's are available, with spin axes parallel to $\hat{\boldsymbol{e}}_1$ and $\hat{\boldsymbol{e}}_2$, respectively. When one RW fails, the coupling effects of the remaining two reaction wheels can influence the angular velocity and attitude of the unactuated axis.

In case of having an underactuated satellite, the spacecraft is known to only be controllable by two wheels in the case of a zero total angular momentum mode, which implies zero initial momentum [48].

$$\boldsymbol{I}\boldsymbol{\omega} + \boldsymbol{h} = 0 \tag{5.7}$$

Under this assumption, the torques generated by the available RW can be treated to control the angular velocity being considered as virtual control inputs.

Euler's rotational equation for the underactuated satellite with two wheels is simply given by

$$\boldsymbol{I}\dot{\boldsymbol{\omega}} = \boldsymbol{u} \tag{5.8}$$

$$\boldsymbol{I}_1\dot{\boldsymbol{\omega}}_1 = M_1 \tag{5.9}$$

$$\boldsymbol{I}_2\dot{\boldsymbol{\omega}}_1 = M_2 \tag{5.10}$$

$$\boldsymbol{I}_3\dot{\boldsymbol{\omega}}_3 = 0 \tag{5.11}$$

where $M_i = -\dot{h_i}$ are the control torques on each axis. Since the total angular momentum of the spacecraft is zero, it can be concluded that the angular momentum on the Z-axis is zero, i.e. $\omega_3 = 0$.

Let considered the quaternion parametrization (See 2.1.2) to describe the attitude of the spacecraft as $\boldsymbol{q} = [q_1, q_2, q_3, q_4]^T = [q_v^T, q_4]^T$

Kinematics are then described as the well-known kinematic differential equations (see [4] chap. (5.5.3))

$$\dot{\boldsymbol{q}}_v = \frac{1}{2}(q_4\boldsymbol{\omega} - \boldsymbol{\omega} \times \boldsymbol{q}) \tag{5.12}$$

$$\dot{q_4} = -\frac{1}{2}(\boldsymbol{\omega}\boldsymbol{q}) \tag{5.13}$$

where $\boldsymbol{\omega}$ is the angular rate. After substituting the zero-momentum condition $\omega_3 = 0$, the kinematic model of the satellite reduces to

$$\begin{aligned}
\dot{q_1} &= \frac{1}{2}q_4\omega_1 - \frac{1}{2}q_3\omega_2 \\
\dot{q_2} &= \frac{1}{2}q_3\omega_1 + \frac{1}{2}q_4\omega_2 \\
\dot{q_3} &= -\frac{1}{2}q_2\omega_1 + \frac{1}{2}q_1\omega_2 \\
\dot{q_4} &= -\frac{1}{2}q_1\omega_1 - \frac{1}{2}q_2\omega_2
\end{aligned} \tag{5.14}$$

Quaternion representation is adopted to avoid any singularities due to the attitude parameterization.

5.2.3 Switching control approach

The control strategy is derived from the principles of the kinematic planning technique described in [69] and it can be seen as as a new approach with interesting similarities with of the control law proposed in [47].

In this case, a switching scheme will be considered, based on the definition of two different desired angular velocity vectors, $\boldsymbol{\omega}_{des_i}$ with $i = 1, 2$..

The threshold of the switching logic from $\boldsymbol{\omega}_{des_1}$ to $\boldsymbol{\omega}_{des_2}$ is determined by a critical value for the dot product $\hat{\boldsymbol{e}}^T\hat{\boldsymbol{b}}$, namely, ϵ_{des}

$$\hat{\boldsymbol{e}}^T\hat{\boldsymbol{b}} \geq \epsilon_{des} \tag{5.15}$$

$$\hat{\boldsymbol{e}}^T\hat{\boldsymbol{b}} < \epsilon_{des} \tag{5.16}$$

The Euler axis can be represented as $\boldsymbol{e} = \dfrac{\boldsymbol{q}_v}{||\boldsymbol{q}_v||}$ thus depends on the attitude and $\boldsymbol{b} = (0\ 0\ 1)$ respect to the body frame, namely, the underactuated direction.

The dot product $\hat{\boldsymbol{e}}^T\hat{\boldsymbol{b}}$ represents a measure of the angular distance between the Euler axis and the undeactuated direction. The switching times depend on whether the Euler axis, at that time instant is sufficiently close to the plane of admissible rotations or not.

The approach consists of a switching logic from two different desired tracking velocities. The first desired angular velocity corresponds to

$$\boldsymbol{\omega}_{des1} = -k_w(\boldsymbol{e}^T\,\boldsymbol{b})\,\frac{\boldsymbol{e}\times\boldsymbol{b}}{||\boldsymbol{e}\times\boldsymbol{b}||} \tag{5.17}$$

the aim of ω_{des1} is to bring the Euler Axis $\hat{\boldsymbol{e}}$ to the plane perpendicular to the underactuated direction $\hat{\boldsymbol{b}}$ when $\hat{\boldsymbol{e}}^T\hat{\boldsymbol{b}} > \epsilon_{des}$. Once the controller reaches the threshold $\hat{\boldsymbol{e}}^T\hat{\boldsymbol{b}} = \epsilon_{des}$, the control law switches and the $\boldsymbol{\omega}_{des2}$ expressed as

$$\boldsymbol{\omega}_{des2} = -k_w\,(\mathbb{I} - \boldsymbol{b}\,\boldsymbol{b}^T)\,\boldsymbol{e} \tag{5.18}$$

Which is equivalent to

$$\boldsymbol{\omega}_{des2} = -k_w\,(\mathbb{I} - \boldsymbol{b}\,\boldsymbol{b}^T)\,\frac{\boldsymbol{q}_v}{||\boldsymbol{q}_v||} \tag{5.19}$$

being $\boldsymbol{q}_v$ the vector part of the quaternion, performing the turn around the non-nominal Euler Axis.

The ω_{des1} is used to stabilise the attitude on the actuated axes ($\hat{\boldsymbol{e}}_1$ and $\hat{\boldsymbol{e}}_2$), and ω_{des2} is used to complete the stabilisation of the unactuated axis ($\hat{\boldsymbol{e}}_3$).

Considering the zero-total angular momentum condition which implies that $\omega_3 = 0$ for the unactuated axis condition, this law will be able to compensate the momentum of the satellite in the unactuated axis with the available reaction wheels in the other two axes. Although the zero-momentum condition is not rigorously conserved under the standard numerical integration (Runge-Kutta), for stability analysis it will be considered that condition instead.

The control law is constructed based on quaternion modeling. This parametrization is more attractive than others (See section 2.1.2) as quaternions are available on-board.

By substituting into the desired tracking angular velocities equations with the quaternions the following expressions are obtained for the case of ω_{des1}

$$\omega_1 = k_w \frac{1}{||\boldsymbol{q}_v||} \frac{q_2 q_3}{q_1^2 + q_2^2} \tag{5.20}$$

$$\omega_2 = -k_w \frac{1}{||\boldsymbol{q}_v||} \frac{q_1 q_3}{q_1^2 + q_2^2} \tag{5.21}$$

$$\omega_3 = 0 \tag{5.22}$$

By substituting the virtual angular velocities w_{des1} and w_{des2} in Eq. (5.14), the closed-loop dynamics on the unactuated axis can be derived and are given by

$$\dot{q_3} = -\frac{1}{2} k_w q_3 \tag{5.23}$$

then $q_3 = q_{30} e^{(-k_w/2)t}$, which means that the attitude component about the unactuated axis converge exponentially to zero.

Moreover, by substituting in 5.14,

$$\dot{q_4} = -\frac{1}{2}q_1\omega_1 - \frac{1}{2}q_2\omega_2 = 0 \tag{5.24}$$

Eq. 5.24 shows that q_4 is constant. Then, considering $q_1^2+q_2^2+q_3^2+q_4^2 = 1$, it follows that

$$q_1^2 + q_2^2 + q_3^2 = C \tag{5.25}$$

As q_4 remains constant, and q_3 decreases exponentially, the sum $q_1^2 + q_2^2$ shall increase with the same rate without diverging, as $q_1^2 + q_2^2 = 1 - q_4^2 - q_3^2$. It can be concluded that the sum is bounded. Singularities are avoided because the numerator exponentially converge to zero faster than the denominator as demonstrated in [18].

Regarding the second desired angular velocity of the switching controller, ω_{des2} (Eq. 5.18) can be represented in terms of quaternion components as

$$\omega_1 = -k_\phi q_1 \tag{5.26}$$

$$\omega_2 = -k_\phi q_2 \tag{5.27}$$

$$\omega_3 = 0 \tag{5.28}$$

By substituting in the kinematics equation one obtains that $\dot{q_3} = 0$ while

$$\dot{q_4} = -\frac{1}{2}q_1\omega_1 - \frac{1}{2}q_2\omega_2 = \frac{1}{2}k_\phi(q_1^2 + q_2^2) \geq 0 \tag{5.29}$$

which is an increasing and monotonic function of time. Therefore, q_4 is increasing and bounded converging when time goes to infinite. This implies the convergence also in $\dot{q_4}$ which implies that $q_1^2 + q_2^2$ converge to zero when time goes to infinity.

5.2.4 Stability analysis

Stability is demonstrated using first, the Multiple Lyapunov Functions (MLF) approach and deriving from these an expression of a common Lyapunov Function for all the switching sequence.

For the control approach proposed, the following result holds.

Lemma 5.2.1 *The switching control law defined by Eqs.5.17 and 5.17 globally asymptotic stabilise the equilibrium* $\boldsymbol{q} = (0, 0, 0, 1)$ *of the system.*

Proof:

Lyapunov stability of switched systems via multiple Lyapunov functions (MLF) can also be used to demonstrate the stability of the nonlinear switching control approach proposed in this thesis (Branicky[70, 71]).

Let be

$$\dot{\boldsymbol{x}} = f(x, u), u = u_i, i \in A \tag{5.30}$$

the system with u_i as control parameter $i : [1, 2]$, thus, the switching signal which is assumed to be a piecewise continuous (from the right) function of time, implying that only a finite number of switches between the two controllers is allowed on any finite-time interval.

$$\begin{cases} i = 1, \hat{\boldsymbol{e}}^T \hat{\boldsymbol{b}} \geq \epsilon_{des} \\ \\ i = 2, \hat{\boldsymbol{e}}^T \hat{\boldsymbol{b}} < \epsilon_{des} \end{cases} \tag{5.31}$$

Lemma 5.2.1 is demonstrated by showing the existence of multiple Lyapunov functions for the system to be controlled, which can be done by picking $V_i = V[\boldsymbol{q}(t)]$ for all $i = 1, 2$.

Let define a Lyapunov function for each switching state, namely V_1 and V_2. For $i = 1$ so that $\hat{\boldsymbol{e}}^T\hat{\boldsymbol{b}} \geq \epsilon_{des}$, and the desired angular velocity is (5.17), a Lyapunov candidate can be

$$V_1 = q_3^2 \tag{5.32}$$

and for $i = 2$ thus when $\hat{\boldsymbol{e}}^T\hat{\boldsymbol{b}} < \epsilon_{des}$, the Lyapunov function is

$$V_2 = q_1^2 + q_2^2 + q_3^2 = 1 - q_4^2 \tag{5.33}$$

Considering the theorems C.0.1 and C.0.2

V_1 and V_2 are both Lyapunov-Like functions and satisfy the Corollary C.0.1.1

During time periods when a mode is inactive, the total energy might be affected by the active mode such that at the next time the inactive mode is activated, the energy exceeds the level attained during it last period of activity. The key idea is to proof for this control approach, and with the Lyapunov functions proposed, that the total energy does not increase, or if it does, the increasing is bounded.

When ω_{des1} is activated, $V_1 = q_3^2$ is monotonically decreasing (exponentially), and when ω_{des2} is activated, $V_2 = q_1^2+q_2^2+q_3^2$. The term q_3^2 decreases and as demonstrated in Eq. 5.29 and considering that $q_1^2 + q_2^2 + q_3^2 + q_4^2 = 1$, $q_1^2 + q_2^2$ converges to zero when time goes to infinity (see Figure. 5.1).

Stability in the sense of Lyapunov is then demonstrated by Theorem C.0.1, and global asymptotic stability by C.0.2 as there exists a function $\gamma > 0$ that satisfies

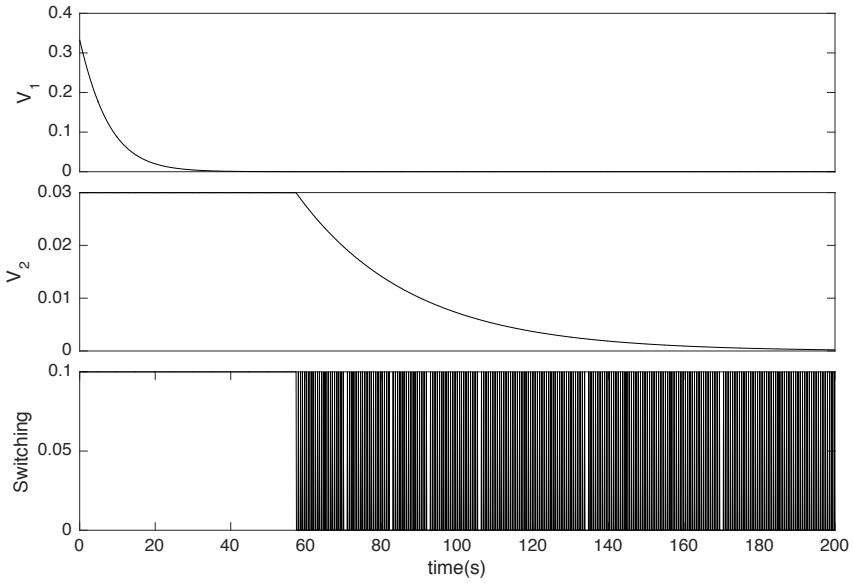

Figure 5.1: Multiple Lyapunov functions

this condition (See Appendix.C)

$$V_{p(t_j)}(x(t_{j+1})) - V_{p(t_i)}(x(t_{i+1})) \leq -\gamma ||\boldsymbol{x}(t_{i+1})||^2 \tag{5.34}$$

Just one Lyapunov function is enough to demonstrate the stability of the whole system. The following Lyapunov function $V_T = V_1 + V_2$,

$$V_T = q_1^2 + q_2^2 + 2q_3^2 \tag{5.35}$$

derived from the previous expressions of V_1 and V_2, fulfil all the requirements to be a common Lyapunov function for all the switching sequence (See Appendix C and figure 5.2).

5.3 Simulation Results

In this section, the effectiveness of the control approach is presented showing the results obtained by the numerical simulations in Matlab/Simulink environment.

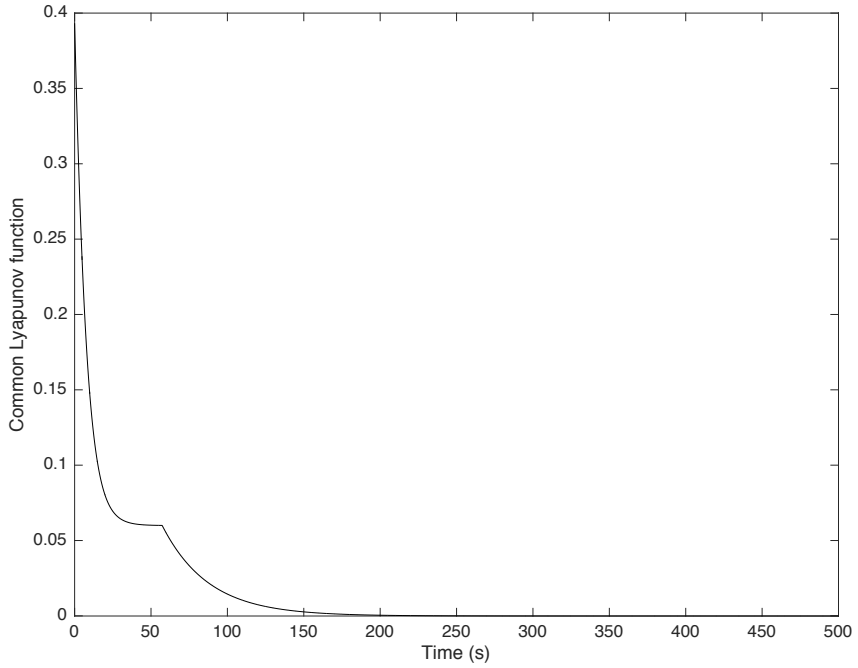

Figure 5.2: One common Lyapunov function for all switching sequences

ESEO [38] satellite main features will be used in the simulations to validate the control approach. Spacecraft data and environment is shown in table 4.1.

A satellite in the course of its nominal operation might be required to perform fast slew manoeuvres. The manoeuvres considered for the simulations are called rest-to-rest, in which the initial and final angular velocity of the satellite is zero. Reaction wheels will also be considered at rest, thus the angular momentum of each reaction wheel is zero. The output control torque of the reaction wheel is bounded by the saturation value, which is the maximum torque a wheel can provide, although some simulations with the non-saturation limit have also been performed.

The performance of the switching controller is shown in two simulation scenarios: one is without in-orbit disturbances and where initial angular velocity is zero (Zero momentum), and the other one is with in-orbit disturbances and the initial angular

velocity is not zero but small (Non-Zero-Momentum).

Except for initial angular velocity and disturbances, the other parameters are the same for all simulations (See Table 4.1). Initial condition values are summarized in Table 5.1.

Three parameters will be considered to compare the performance of the control laws, namely, settling time, maximum torque and integrated torque. This is a value that represents the total amount of torque that wheels require performing a certain manoeuvre. The expression for the integrated torque is,

$$U_t = \int_0^T ||\boldsymbol{g}||dt \tag{5.36}$$

where $\boldsymbol{g} = (g_1, g_2, g_3)$ is the torque provided by the wheels and T is the time considered for the manoeuvre. In this case, $g_3 = 0$ as the third wheel is not available.

In both cases, convergence time, integrated torque and maximum torque per axis have been shown and considered as design parameters to evaluate the performance of the control law.

Table 5.1: Manoeuvre studied

Sample manoeuvre		
CASE 2.1: Initial Conditions	$\boldsymbol{\omega}_0$	$(0, 0, 0)^T$ rad/s
	$\boldsymbol{q}_0$	$(0.1, 0.1, 0.1, 0.9849)^T$
Gains chosen (rad/s)		
Discontinuous Horri et al. control law	$g = 0.33$ $k = 0.02$	
Switching control law	$k_\omega = 0.15$ $k_\phi = 0.06$	

Montecarlo Analysis has been chosen as computational algorithm. Simulations have been performed for the same set of random initial conditions in order to assess the performance and to select the control gains.

5.3.1 Epsilon selection

A thousand random values for the initial quaternion have been considered for this set of simulations. The goal was the selection of a ϵ_{des} for the best performance. The study was based in testing the influence of ϵ_{des} while keeping the same k_ϕ and k_ω, ratio. The results show that in terms of settling time, there is a minimum for a certain ratio. That minimum is reduced as the value of the ratio is reduced. The integrated torque increases while increasing ϵ_{des}, thus, the minimum settling time can be considered as an upper bound for each ratio. The value chosen for the following simulations is upper bounded by $\epsilon_{des} = 0.37$, the epsilon chosen is: ϵ_{des}=0.05 after a trade off between integrated torque and settling time.

5.3.2 Switching behaviour

The switching controller will be considered as the following system

$$\dot{\boldsymbol{x}} = f(x, u), u = u_i, i \in A \tag{5.37}$$

where $x \in \mathbb{R}^n$ is the state, u the control input, $u_i, i \in A$ are the candidate controllers and $i : [1, 2] \in A$ are the switching signals.

Let u_1 be ω_{des1} and u_2 be ω_{des2}.

The control law switches from u_1 to u_2 and vice versa. The first switching corresponds with u_1, and it is the longer respect to the successive switchings until

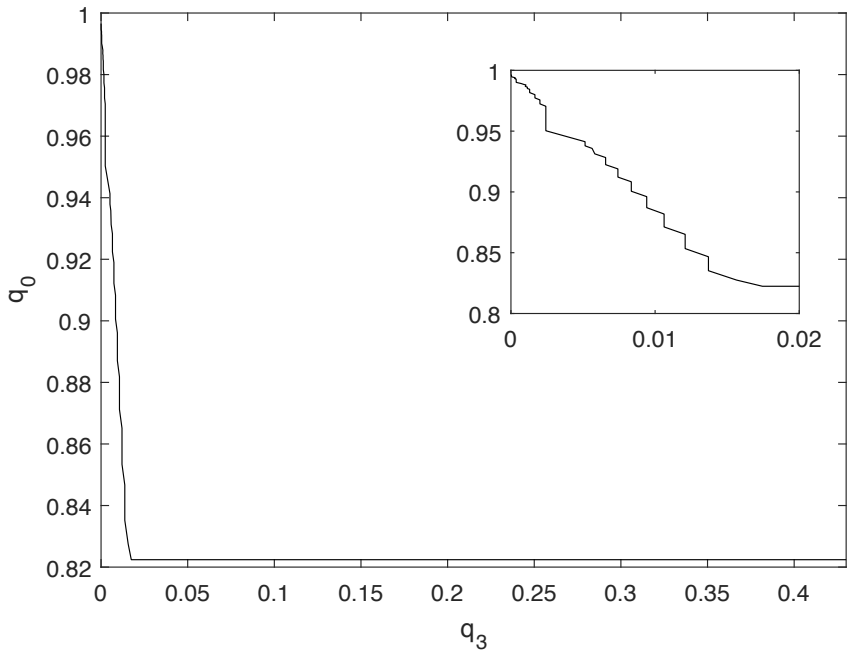

Figure 5.3: Switching behaviour

the convergence. Figure 5.3 shows the switching behaviour represented by a phase diagramme of q_3 and q_0 and the influence of ϵ_{des} in the switching behaviour.

5.3.3 Zero total angular momentum

The first simulation is carried out under the conditions that there is no environmental disturbances and the initial angular velocity is zero (Case 2.1, 2.2). This corresponds with the quite ideal assumption that the total angular momentum of the whole satellite is zero, (See section 3.3).

Simulation results for the Case 2.1 are shown in Fig. 5.5, in which this controller can render a stable closed-loop system with both the underactuated and the actuated axes asymptotically stabilised from a non-zero initial attitude to the equilibrium

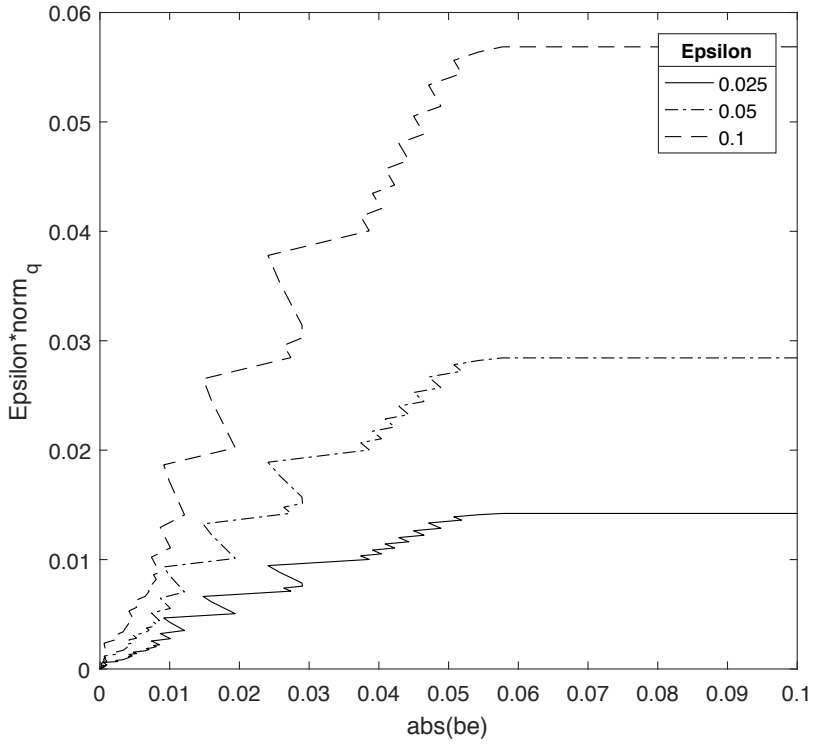

Figure 5.4: Epsilon influence in the switching behaviour

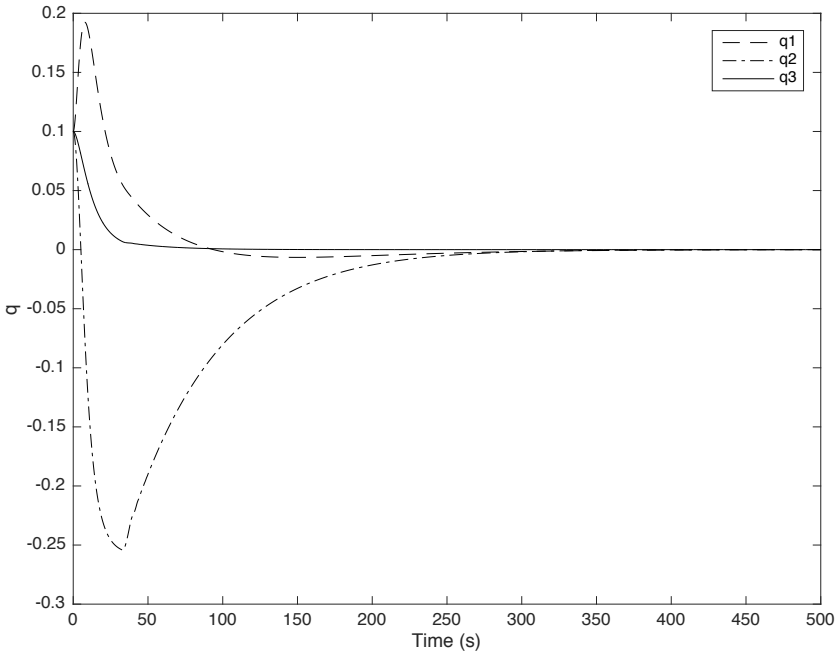

Figure 5.5: Attitude representation for the zero momentum case

$\boldsymbol{q} = (0\ 0\ 0\ 1)$ within 0.02 orbits. Saturation limits of the wheels will not be considered for this case .

5.3.4 Non-zero total angular momentum including disturbances

The second set of simulations are carried out considering a more realistic scenario, also for the case 2.1.

Considering a no-zero initial angular velocity ($\omega_0 = (0.001\ 0.001\ 0.001)\ rad/s$) and in-orbit disturbances. These are: gravity gradient, solar radiation pressure, atmospheric drag, and residual magnetic dipole. Uncertainties in the inertia matrix have also been included and a non-zero initial angular velocity to validate the robustness of the control law.

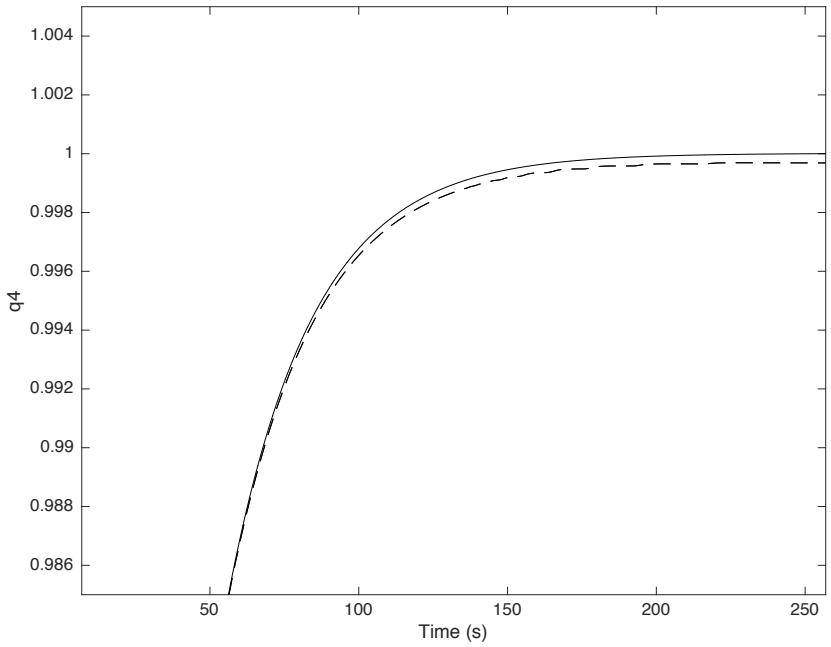

Figure 5.6: q4 - Zero momentum VS non-zero momentum case

In order to compare settling times, simulations are stopped when the attitude q_4 term reaches a value such that the total error is 10^{-4}.

If the simulation lasts for a longer time, higher pointing accuracy is achieved. The attitude can converge to a small area around zero with time. This switching approach shows a good performance in terms of pointing accuracy against disturbances and uncertainties.

The control law performs well in the case of non-zero-momentum, as the attitude converges (See Fig. 5.6). The effect of the non-zero momentum (discontinuous line) is seen in the settling time. Time needed to converge is a 12.99% higher respect to the zero-momentum case (continuous line) and the total integrated torque is 3% higher.

5.3.5 Actuators saturation effects

For the initial set of simulations, the saturation of the wheels was not considered validating the control law in a non-limited approach. In order to visualise the maximum torque that would be required.

Saturation limits are now included. In Fig 5.7, it is shown a comparison of q4 values for the zero momentum case. The continuous line represents the non-saturated case, while the discontinuous one represents q4 in the case in which a limit of $h_w = 0.01$ is considered, which corresponds with the maximum wheel torque (per axis) for the ESEO nanosatellite (See Table 4.1) performing the manoeuvre (Case 2.1). This value has been chosen as saturation value for the simulations, which is the maximum torque a single wheel can provide.

The problem has been studied for different manoeuvres, both for zero-momentum and small non-zero momentum. The saturation limit is reached by the wheels in all cases.

For the zero momentum case, simulations show that settling time increases respect to the non-saturated case, for this manoeuvres the increase represents a $10,74\%$, while total integrated torque decreases an 11.12% for the zero-momentum case. Results show that settling time increases respect to the non-saturated case, for this manoeuvre the increase represents a 5.1%, while total integrated torque decreases an 11.43%. It can be concluded that the controller performs well also when actuators saturate.

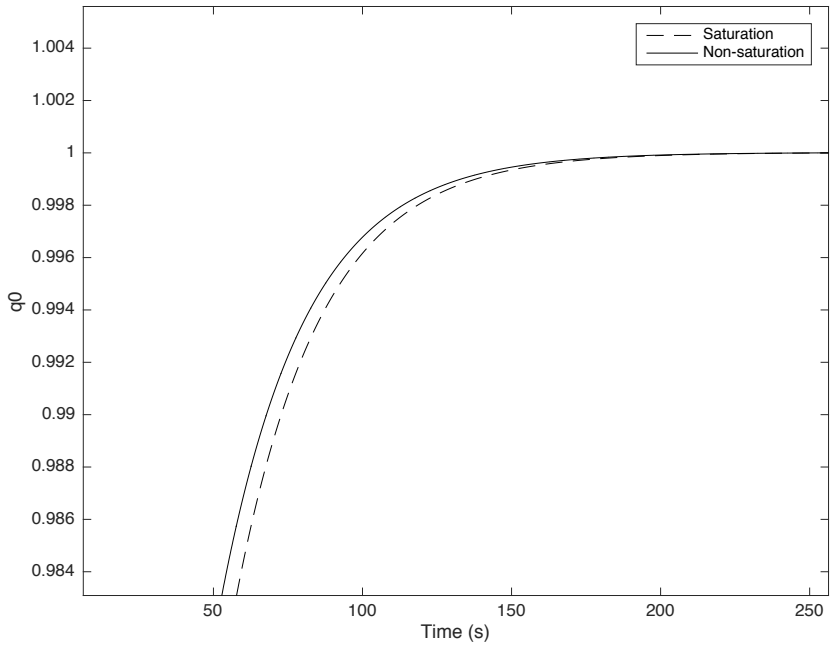

Figure 5.7: q4 - Zero momentum case, saturation Vs non-saturation

5.3.6 Comparison between controllers

The discontinuous controller in [47] is compared with the switching control approach proposed. Horri et al. control law is expressed by

$$\omega_{d1} = -kq_1 + g\frac{q_2 q_3}{q_1^2 + q_2^2} \tag{5.38}$$

$$\omega_{d2} = -kq_2 - g\frac{q_1 q_3}{q_1^2 + q_2^2} \tag{5.39}$$

$$\omega_3 = 0 \tag{5.40}$$

It comes out that the analytical representation in terms of quaternion, for both controllers differs in the switching, that the novel approach proposes, between the two terms of 5.38 and 5.39. The results of the numerical simulations show that the advantage of using this approach, is such that for the same total integrated

torque, the settling time and maximum torque per axis are lower for a set of initial conditions of the switching control law.

Different simulations have been performed for the two initial conditions shown in Table 5.1. Continuous lines in all the figures of this section represent the Switching controller whereas the discontinuous lines represent the Horri et al. approach.

Figure 5.8 (Case 2.1) shows the attitude profiles in terms of quaternion representation of an underactuated satellite using the discontinuous control law in [47] and the switching control law proposed in Eq.(5.17) and Eq.(5.18) for the case of non-zero momentum. Figure 5.9 shows attitude convergence for the zero momentum case.

It can be seen from the plots that attitude about all the axes were stabilized to equilibrium position faster using the switching control law.

Gains chosen for both controllers are such that the total integrated torque is the same. The settling time and maximum torques obtained are in Table 5.2.

It can be concluded that for the same integrated torque the settling time is a 35.2% higher for the Horri et al. (See q4 plot in Fig. 5.10) controller and also the values of the maximum torque are higher (See Fig. 5.11). Thus, a better performance is shown by the switching controller proposed in this thesis.

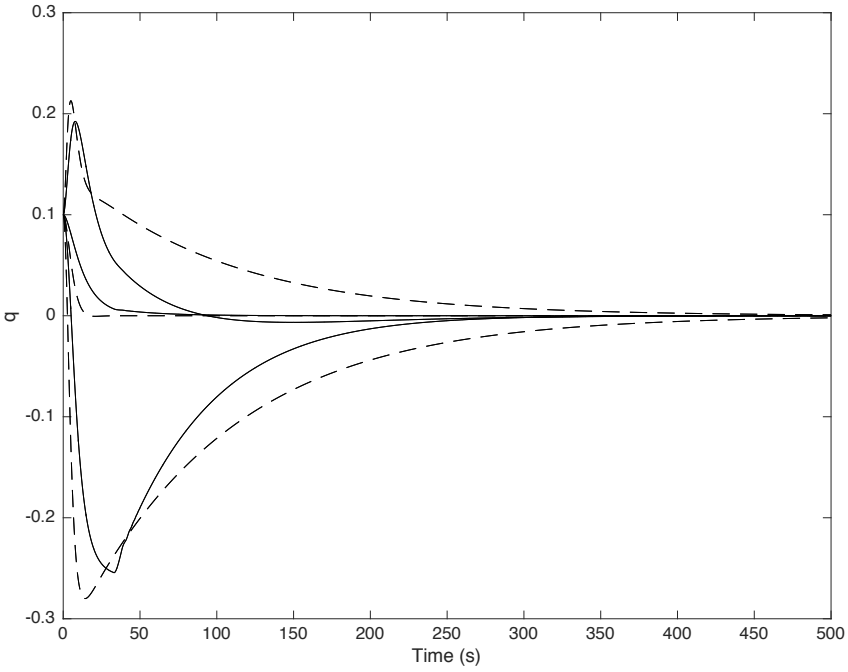

Figure 5.8: Attitude representation in quaternions for the case 2.1 - Non-zero momentum

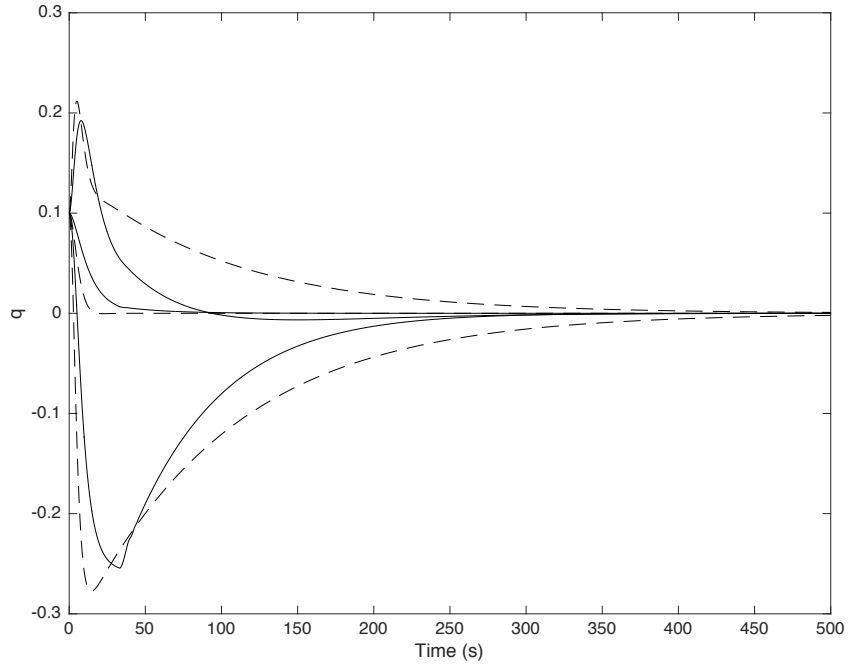

Figure 5.9: Attitude quaternions Horri et al. Vs Switching law - Zero Momentum

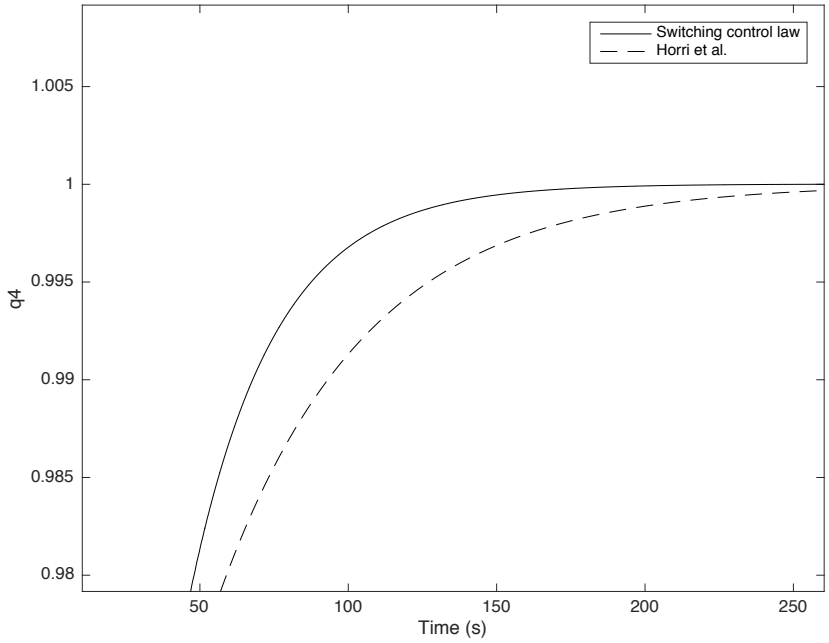

Figure 5.10: q4 (Horri et al. Vs Switching law) zero momentum case

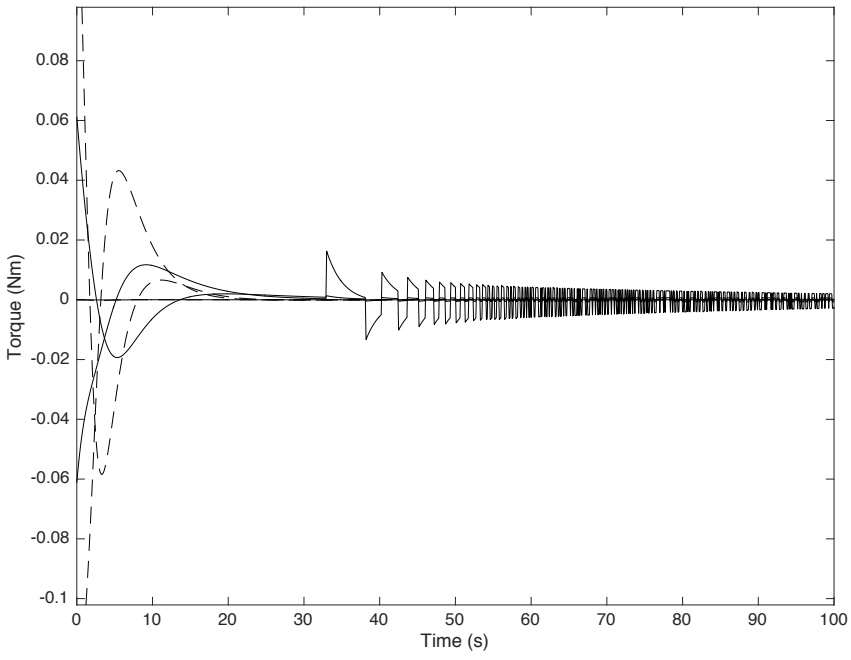

Figure 5.11: Wheels torque - Horri et al. Vs Switching law - zero momentum

Table 5.2: Controllers comparison

Parameter	**Horri**	**Switching control**	**Units**
Integrated torque	0.71	0.71	Nms
Settling time	205	133	s
Maximum torque	(0.158 0.043 0.0000)	(0.061 0.016 0)	Nm

Chapter 6

Conclusions

In this thesis two different cases involving spacecraft three–axis attitude stabilisation have been presented.

In the Case 1, the combined use of magnetic and mechanical control laws is proposed to achieve the attitude stabilisation in the orbit frame by means of three mutually orthogonal magnetic actuators providing continuous momentum dumping and a set of three orthogonal reaction wheels for attitude control. A formal proof of convergence is also provided, highlighting the role of the variability of the magnetic field along the orbit plays an important role in the proof of asymptotic stability of the system toward the equilibrium point.

In particular, global exponential stability is proven for the closed-loop system where angular momentum management is obtained by means of magnetic actuation. The system stability proof for the whole cascade, represents the additional contribution of the present thesis. The results hold for many practical applications regarding small-scale spacecraft.

Simulation results are presented in order to demonstrate the effectiveness of the

control laws and validate the theoretical results. As a further contribution, the control laws are shown to perform well in the presence of external disturbances, spacecraft inertia matrix uncertainties, and control implementation issues such as actuator saturation, control quantization, and measurement noise.

Case 2 addresses the problem of three–axis stabilisation within underactuated conditions. Although most spacecraft are equipped with redundant reaction or momentum wheels, research on underactuated attitude control is advantageous as failures of both primary and secondary reaction wheels are possible throughout a mission. Different solutions have been proposed over the years, such as using thrusters to mitigate the issue, including more redundant actuators, etc. However, these solutions present some disadvantages. The use of thrusters would involve undesired fuel consumption and including more actuators might not be feasible in terms of mass budget. As an alternative, in this thesis, full 3-axis control can still be achieved, using the two remaining reaction wheels from a standard orthogonal 3-wheel configuration using the switching control approach proposed.

As proved mathematically, the control law proposed stabilises the underactuated system in terms of Lyapunov. The numerical simulations show that the control law performs well in terms of settling time and pointing accuracy, in the case of ideal zero-momentum and including in-orbit disturbances and model uncertainties. This results an important improvement as main problem with existing underactuated attitude control designs is their limited capabilities against disturbances while performing slew manoeuvres.

The control law proposed is compared with the previous result of Horri et. al showing a better performance in terms of settling time and maximum torque. [47]

For both Case 1 and Case 2, good performance and stability is proven to reach

three-axis stabilisation. These control approaches are potential candidates to be used for satellite missions scenarios as the ones described in this thesis.

6.1 Future Work

Hybrid systems, that included both magnetic and mechanical actuation are given encouraging results to the AOCS open issues as demonstrated in Case 1.

Further investigations on the switching control law are planned. In Case 2, the switching control approach might be enhanced considering the contribution of three magnetic torques, that could provide a better performance if included in the AOCS subsystem. One interesting aspect is to more deeply investigate the system uncertainties. Another work could be on the suitability for large angle manoeuvre problem. In addition, the evaluation of control efforts and a study on the improvement using specific control methods to mitigate the effect of uncertainties such as adaptive control and are also of interest for the future.

Publications

Overview of AOCS for Nanosatellites and Expected Short Term Evolution. De Angelis, E. L., Giulietti, F., Modenini, D., Serrano Castillo, E., Tortora., P., University of Bologna, Italy,10th IAA Symposium on Small Satellites for Earth Observation, Berlin. April 2015, 20th-24th.

Magnetic and mechanical attitude control approaches for three-axis stabilized nano satellites. Serrano Castillo, E., Giulietti, F., and de Angelis, E. L., University of Bologna, Italy. 4S Small Satellites Systems and Services, ESA Conference. La Valleta (Malta) 29th May -4th June 2016.

Appendix A

Case 1: Proof of Lemma 1

Global exponential stability of the origin $\boldsymbol{Z} = \mathbf{0}$ for the nominal system

$$\dot{\boldsymbol{Z}} = -\left[\boldsymbol{T}_{BI}^{T}\left(\mathbb{I}_3 - \hat{\boldsymbol{b}}\,\hat{\boldsymbol{b}}^{T}\right)\boldsymbol{T}_{BI}\right](k_\zeta\,\boldsymbol{Z}) \tag{A.1}$$

is provided by the following corollary.

Corollary A.0.0.1 *Consider a nonlinear non–autonomous dynamic system* $\dot{\boldsymbol{x}} = \boldsymbol{f}(t, \boldsymbol{x})$*, where* $\boldsymbol{f} : \mathbb{R}^n \times \mathbb{R} \to \mathbb{R}^n$ *is piecewise continuous in* t *and Lipschitz in* $\boldsymbol{x}$*. Let* $\boldsymbol{x} = \mathbf{0}$ *be an equilibrium point for the system at* $t = 0$*. Also assumimg that a strictly positive definite Lyapunov–like function* $V(\boldsymbol{x}) > 0$ *exists, where (i)* $V : \mathbb{R}^n \to \mathbb{R}$ *is a smooth scalar function of the state* $\boldsymbol{x}$ *only and (ii) its gradient vanishes at the origin only, that is,* $\nabla_x V = \mathbf{0}$ *at* $\boldsymbol{x} = \mathbf{0}$ *and* $\nabla_x V \neq \mathbf{0}$ *elsewhere. If the Lyapunov–like function* $V(\boldsymbol{x})$ *and its time derivative* $\dot{V}(t, \boldsymbol{x})$ *satisfy the conditions:*

1. $k_1 \,||\boldsymbol{x}||^c \leq V(\boldsymbol{x}) \leq k_2 \,||\boldsymbol{x}||^c \qquad k_1 > 0, k_2 > 0, c > 0$*;*
2. $\dot{V}$ *is negative semi–definite, that is,* $\dot{V}(t, \boldsymbol{x}) \leq 0$*;*

3. $\dot{V}$ is uniformly continuous;

4. the iso-surfaces S of $V(\boldsymbol{x})$ in the state space $\mathbb{R}^n$ do not contain any integral curves $\boldsymbol{x}(t)$ of the vector field $\boldsymbol{f}$ other than the constant ones ($\boldsymbol{x}(t) = \boldsymbol{x}_e,\ \forall t$);

then the state converges to one of the (at least locally) stable equilibria. If the origin is the only equilibrium, it is globally exponentially stable.

Proof: Since the Lyapunov candidate function V only depends on the state $\boldsymbol{x}$ one has:

$$\dot{V}(t, \boldsymbol{x}) = \lim_{\delta t \to 0} \frac{V(\boldsymbol{x}(t+\delta t)) - V(\boldsymbol{x}(t))}{\delta t} = \nabla_x V\, \boldsymbol{f}(t, \boldsymbol{x}) \tag{A.2}$$

Since the iso-surfaces S of $V(\boldsymbol{x}(t))$ do not contain any integral curves of $\boldsymbol{f}$, the right hand term cannot be zero if an equilibrium point is not reached. Thus, for all $t > 0$ the quantity

$$V(\boldsymbol{x}(t+\delta t)) - V(\boldsymbol{x}(t)) = \int_t^{t+\delta t} \nabla_x V\, \boldsymbol{f}(\tau, \boldsymbol{x}(\tau, \boldsymbol{x}))\, d\tau < 0 \tag{A.3}$$

is a finite negative term, and there exists a $0 < \lambda < 1$ such that

$$V(\boldsymbol{x}(t+\delta t)) - V(\boldsymbol{x}(t)) < -\lambda\, V(\boldsymbol{x}(t)). \tag{A.4}$$

From this point onwards the proof follows that of Theorem 8.5 in [72].

By choosing the Lyapunov candidate $V(\boldsymbol{Z}) = 1/2\, \boldsymbol{Z}^T\, \boldsymbol{Z}$, system (A.1) satisfies Conditions 1, 2, and 3, with $\dot{V}(t, \boldsymbol{Z}) = -k_h\, \boldsymbol{Z}^T \left[\boldsymbol{T}_{BI}^T \left(\mathbb{I}_3 - \hat{\boldsymbol{b}}\, \hat{\boldsymbol{b}}^T \right) \boldsymbol{T}_{BI} \right] \boldsymbol{Z}$. In case of torque–free motion, the nominal system (A.1) reduces to $\dot{\boldsymbol{Z}} = \boldsymbol{0}$, with the result that $\boldsymbol{Z}$ remains fixed in the inertial frame. Conversely, the Earth magnetic field is time–varying, so that the trajectory $\boldsymbol{Z}(t) = \|\boldsymbol{Z}\|\, \hat{\boldsymbol{b}}(t)$ cannot be a solution for the nominal system (A.1). Thus, also Condition 4 is satisfied and the origin $\boldsymbol{Z} = \boldsymbol{0}$ is exponentially stable.

Appendix B

Gains Study

A gains-selection study has been performed to identify the effect of the values of the gains in the settling time, integrated torque and maximum torque.

The following figures represent the isolines which show the same value of a certain parameter in the plane of the k_ϕ and k_ω.

Three manoeuvres have been analysed:

Table B.1: Manoeuvres studied

Sample manoeuvre			
CASE 2.1B: Initial Conditions	$\boldsymbol{\omega}_0$	$(0,\ 0,\ 0)^T$	rad/s
	$\boldsymbol{q}_0$	$(0.1,\ 0.1,\ 0.1,\ 0.9849)^T$	
CASE 2.2B: Initial Conditions	$\boldsymbol{\omega}_0$	$(0,\ 0,\ 0)^T$	rad/s
	$\boldsymbol{q}_0$	$(0.5,\ 0.5,\ 0.1,\ 0.7)^T$	
CASE 2.3B: Initial Conditions	$\boldsymbol{\omega}_0$	$(0,\ 0,\ 0)^T$	rad/s
	$\boldsymbol{q}_0$	$(0.1,\ 0.1,\ 0.5,\ 0.8544)^T$	

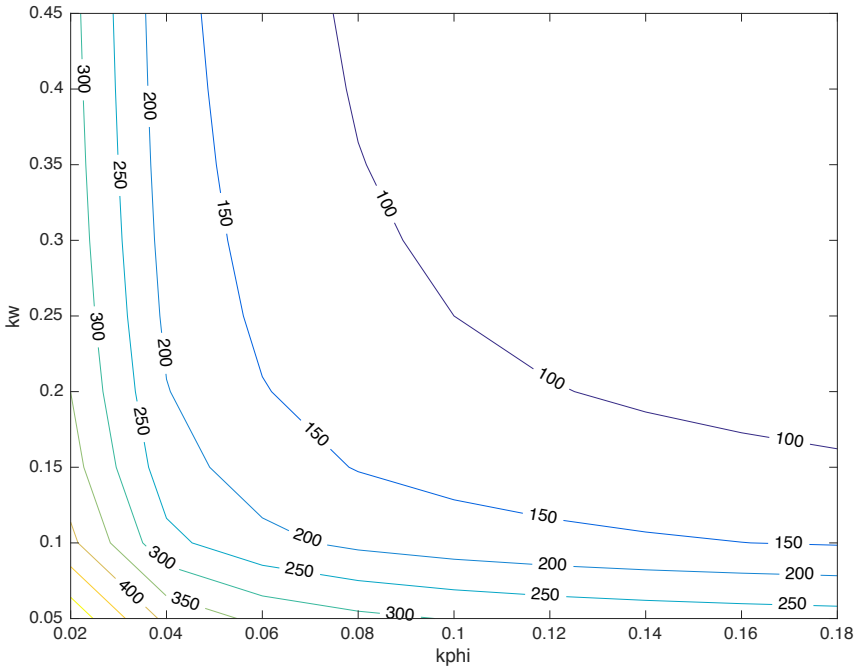

Figure B.1: Convergence time Case 2.2B

In terms of convergence time, graphs for each of the three cases show that increases in k_ϕ and k_ω, reduce the settling time. For small values of k_ϕ, k_ω has a negligible influence and vice versa.

The integrated torque shows different behaviour depending on the manoeuvre performed. For the Case 2.1B (Fig. B.2 from zero to $k_\phi = 0.1$ and $k_\omega = 0.35$ the integrated torque increases almost linearly. For values over $k_\phi = 0.1$, the increase of k_ω over $k_\omega = 0.2$ does not produce an increase in the integrated torque. For small values of $k_\omega$instead, an increase in k_ϕ does not affect to the integrated torque. In Fig. B.3 it can be seen for the case 2.2B that for small values of k_ϕ, an increase in k_ω, does not produce a great change in the integrated torque and vice versa. In case 2.3B, the integrated torque remains almost constant while increasing k_ω for a certain value of k_ϕ and increases as k_ϕ increases.

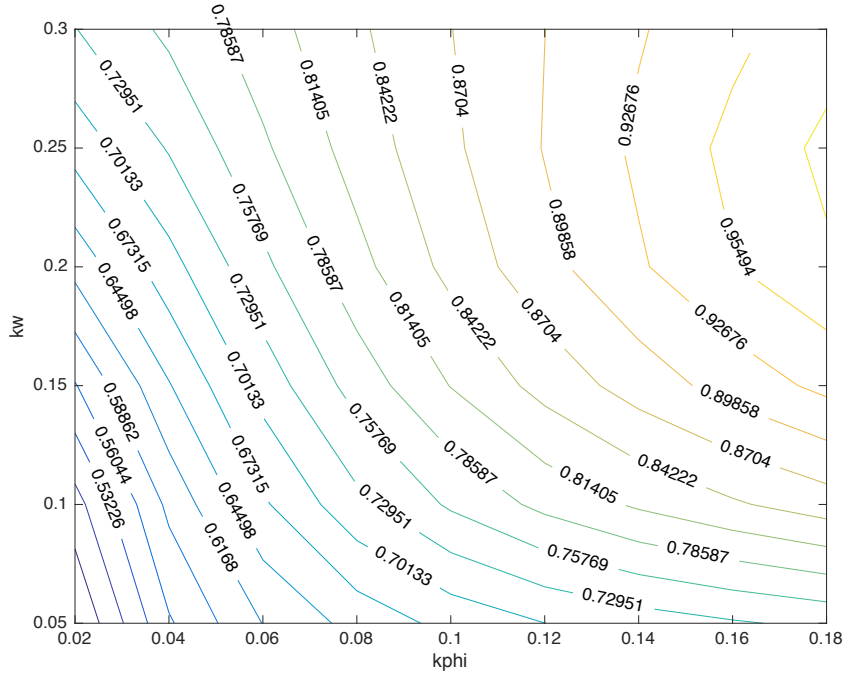

Figure B.2: Integrated torque Case 2.1B

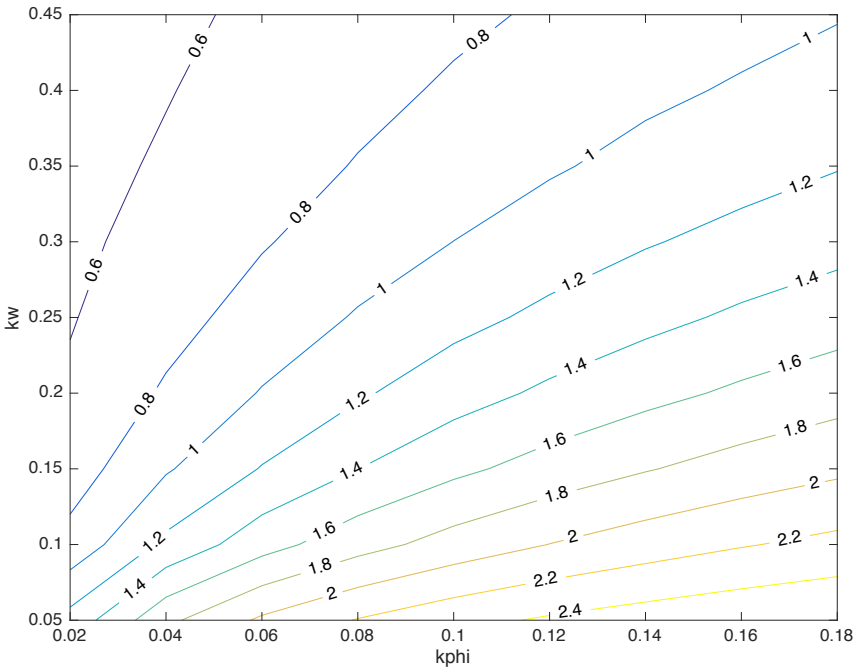

Figure B.3: Integrated torque Case 2.2B

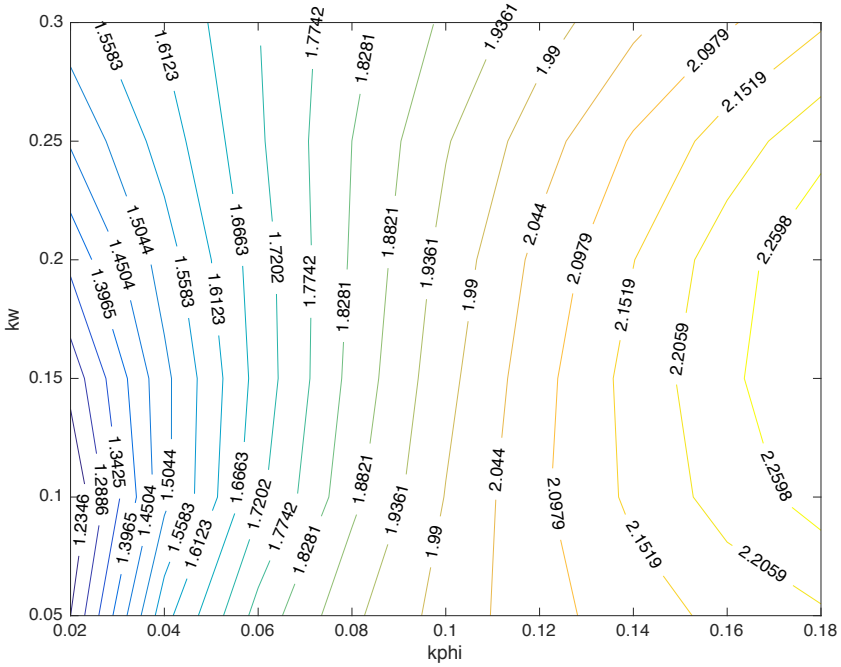

Figure B.4: Integrated torque Case 2.3B

The maximum torque has an almost constant behaviour. For a certain value of k_ω, the maximum torque does not vary increasing k_ϕ as seen in Fig. B.5.

In conclusion, these figures can be used for the gains selection depending on mission requirements and result useful in trade-off studies to choose the best the performance of the switching control law.

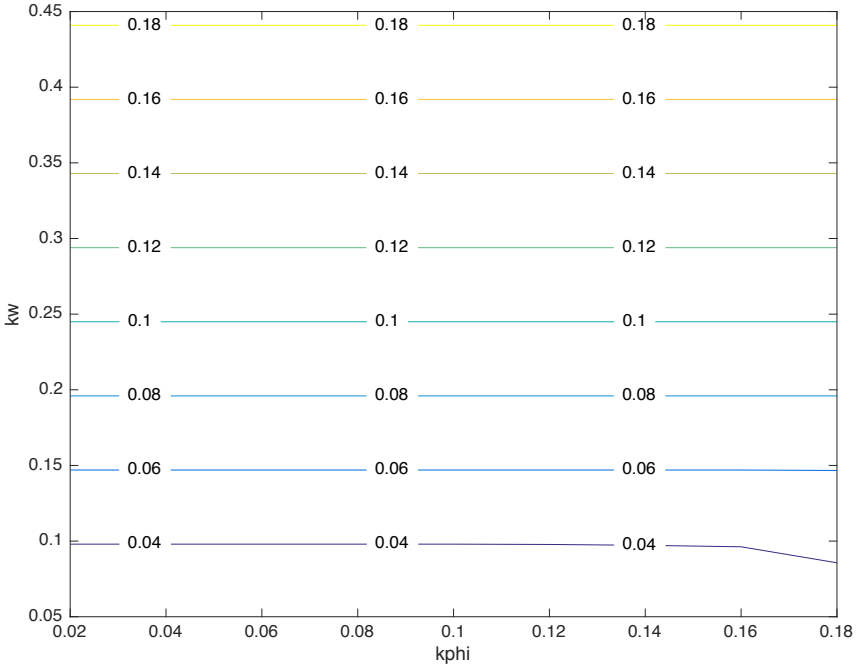

Figure B.5: Maximum Torque Case 2.1B

Appendix C

Case 2: Stability proof - Multiple Lyapunov Approach

Classical Lyapunov stability theory shows that stability depends on the existence and/or construction of an appropriate (continuous and differentiable) Lyapunov function which may not exist or, when it does, may be difficult to construct. [73].

In general, the stability of subsystems do not imply the stability of the switched system under arbitrary switching, and a switched system may be stable for a switching signal even if all subsystems are unstable. To deal with the problem of arbitrary switching when all subsystems are stable, the stability is reached if a common Lyapunov function is found.

For hybrid systems, it might be not obvious to demonstrate the stability by one Lyapunov function. Yet, the intrinsic discontinuous nature of a hybrid system strongly suggests using Multiple Lyapunov Functions (MLFs) concatenated together to produce a non–traditional (piecewise continuous and piecewise differentiable) Lyapunov function.

In this framework results from [71, 70, 73] will be used to demonstrate the stability of the control approach described in Chapter 5.

A switched system can be modelled in general as

$$\dot{x}(t) = f_i(x(t)), i \in \{1, ..., M\} \tag{C.1}$$

where $x(t) \in \mathbb{R}^n$ is the state and i the switching signal. Let define a controller switching as a system with single dynamics and multiple controllers, which results in a switching system.

$$\dot{\boldsymbol{x}} = f(x, u), u = u_i, i \in A \tag{C.2}$$

where $x \in \mathbb{R}^n$ is the state, u the control input, $u_i, i \in A$ are the candidate controllers and $i : [0, \infty)$ with A as switching signal.

The controller proposed in Chapter 5 is classified as state-dependent, which means that $u_i = u_i(x)$.

Considering the following assumptions

Assumption 4 *Each f_i is globally Lipschitz continuous.*

Assumption 5 *There are finite switches in finite time.*

and defining a switching sequence

$$S = xo; (i_0, t_0), (i_1, t_1)...(i_n, t_n) \tag{C.3}$$

for $i_n \in M$ with its associated projection sequences. The switching sequence completely describes the trajectory of the system according to the following rule

(i_k, j_k) which means that the system evolves according to $\dot{\boldsymbol{x}}(t) = f_{i_k}(x(t), t)$ for $t_k \leq t < t_{k+1}$.

Considering the Theorem 8.14 in [70] Stability is demonstrated by the following theorem

Theorem C.0.1 *Suppose there exists $i = 2$ candidate Lyapunov functions $V_i = V(\boldsymbol{q}, i)$ and vector fields as Equation* (C.1) *with $f(0, i) = 0$, for each $i \in M$. Moreover, $V : \mathbb{R}^n \times K \to \mathbb{R}_+$ is continuous. Let S be the switching sequences associated. If for each $S \in S$ and for all i, V_i is Lyapunov-like function for f_i $x_s(\cdot)$ over S, i and the V_i satisfy the sequence non-increasing condition for $x_s(\cdot)$, then the system is stable in the sense of Lyapunov.*

where the sequence non-increasing condition for a trajectory $x(\cdot)$ is satisfied if

$$V_{i_{j+1}}(x(t_{j+1})) < V_{i_j}(x(t_j)) \tag{C.4}$$

if there are candidate Lyapunov functions V_i corresponding to f_i for all i, where $t_{i,k}$ denotes the $k-th$ time that vector field f_i is switched in, which in other words, means that V_i decreases on each interval when the i-th subsystem is active.

The definition considered for Lyapunov-Like function is shown in Corollary C.0.1.1.

Corollary C.0.1.1 *Consider a nonlinear system $\boldsymbol{f}_i(\boldsymbol{x}) = \boldsymbol{A}_i\boldsymbol{x}$, briefly define a family of Lyapunov-Like functions $(V_i, i = 1, ..., M)$ each associated with the vector field $\boldsymbol{f}(\boldsymbol{x}, i) = \boldsymbol{f}_i(\boldsymbol{x})$. A Lyapunov-Like function for the system $\dot{\boldsymbol{x}} = \boldsymbol{f}_i(\boldsymbol{x})$ point is a real-valued function $V_i(x)$ defined over the region Ω_i which satisfies the conditions:*

1. *Positive definiteness $V_i(\boldsymbol{x}) > 0$ and $V_i(\boldsymbol{x}) = 0$ at the equilibrium point.*

2. $\dot{V}$ is negative semi–definite, that is, $\dot{V}(t, \boldsymbol{x}) \leq 0$;

Using Multiple Lyapunov-Like Functions to form a single non-traditional Lyapunov function offers much greater freedom and infinitely more possibilities for demonstrating stability, for constructing a non-traditional Lyapunov function, and for achieving the stabilization of the hybrid system which we now restrict to the special (autonomous) form where

$$\dot{\boldsymbol{x}}(t) = f(x(t), p(t)) = f_{p(t)}((x(t)) \tag{C.5}$$

where $p(t) \in \{1, ...M\}$ And being $p(t)$ piecewise continuous, implying that there are only a finite number of switches per unit time [73].

Following the Theorem 3.2 in [73], given the M-switched non linear system in (C.5), supposing that each f_i has an associated Lyapunov-like function V, in the region Ω_i, each with equilibrium point $\boldsymbol{x} = 0$ and suppose that $\bigcup_i \Omega_i = \mathbb{R}^n$. Let p(t) be the switching sequence such that p(t) can take on the value i only if $x(t)$ $\in \Omega_i$ and in addition

$$V_i(x(t_{i,k})) < V_i(x(t_{i,k-1})) \tag{C.6}$$

where $t_{i,k}$ denotes the $k - th$ time that vector field f_i is switched in. Then (C.5) is stable.

Global asymptotic stability of the system C.5 is given by Theorem 3.1 in [73] and the following is applied to Case 2 in Chapter 5.

Theorem C.0.2 *For $i < j$, $t_i < t_j$ be switching times for which $p(t_i) = p(t_j)$ and suppose there exists $\gamma > 0$ such that*

$$V_{p(t_j)}(x(t_{j+1})) - V_{p(t_i)}(x(t_{i+1})) \leq -\gamma ||\boldsymbol{x}(t_{i+1})||^2 \tag{C.7}$$

it follows that system (C.5)*, with* $f_{p(t)}(x) = A_{p(t)}x$ *and switching function* $p(t)$*, is globally asymptotically stable (GAS).*

References

[1] James R Wertz. *Spacecraft attitude determination and control*, volume 73. Springer Science & Business Media, 2012.

[2] Hank Heidt, Jordi Puig-Suari, Augustus Moore, Shinichi Nakasuka, and Robert Twiggs. Cubesat: A new generation of picosatellite for education and industry low-cost space experimentation. 2000.

[3] Bill Doncaster, Jordan Shulman, and Williams Caleb. Spaceworks' 2017 nano/microsatellite market forcast. 2017.

[4] Bong Wie. *Space vehicle dynamics and control*. Aiaa, 1998.

[5] James Diebel. Representing attitude: Euler angles, unit quaternions, and rotation vectors. *Matrix*, 58(15-16):1–35, 2006.

[6] Bong Wie, H Weiss, and A Arapostathis. Quarternion feedback regulator for spacecraft eigenaxis rotations. *Journal of Guidance, Control, and Dynamics*, 12(3):375–380, 1989.

[7] EL de Angelis and F Giulietti. Unified kinematic framework for a non-nominal euler axis/angle rotation. *Acta Astronautica*, 116:333–338, 2015.

[8] Jack B Kuipers et al. *Quaternions and rotation sequences*, volume 66. Princeton university press Princeton, 1999.

[9] James Richard Wertz, David F Everett, and Jeffery John Puschell. *Space mission engineering: the new SMAD*. Microcosm Press, 2011.

[10] Erwan Thébault, Christopher C Finlay, Ciarán D Beggan, Patrick Alken, Julien Aubert, Olivier Barrois, Francois Bertrand, Tatiana Bondar, Axel Boness, Laura Brocco, et al. International geomagnetic reference field: the 12th generation. *Earth, Planets and Space*, 67(1):1–19, 2015.

[11] Jasper Bouwmeester and J Guo. Survey of worldwide pico-and nanosatellite missions, distributions and subsystem technology. *Acta Astronautica*, 67(7):854–862, 2010.

[12] Scott R Starin and John Eterno. Attitude determination and control systems. 2011.

[13] Emanuele L de Angelis, Fabrizio Giulietti, Anton HJ de Ruiter, and Giulio Avanzini. Spacecraft attitude control using magnetic and mechanical actuation. *Journal of Guidance, Control, and Dynamics*, 38(11):564–573, 2015.

[14] Charles Swenson, Chad Fish, Erik Stromberg, Bryan Bingham, and Phillip ANDERSON. The international space station as a launch platform for cubesats to study space weather. In *Proceedings of the 3rd Nanosatellite Symposium, Kitakyushu, Japan*, 2011.

[15] https://eoportal.org/web/eoportal/home. Earth observation directory and news - eoportal. 2017.

[16] Ali Siahpush and Janet Gleave. A brief survey of attitude control systems for small satellites using momentum concepts. 1988.

[17] Cornelius J Dennehy. Spacecraft hybrid (mixed-actuator) attitude control experiences on nasa science missions. 2014.

[18] Nadjim Mehdi Horri, Phil Palmer, and Stephen Hodgart. Practical implementation of attitude-control algorithms for an underactuated satellite. *Journal of Guidance, Control, and Dynamics*, 35(1):40–45, 2012.

[19] Roger W Brockett et al. Asymptotic stability and feedback stabilization. *Differential geometric control theory*, 27(1):181–191, 1983.

[20] Peter Crouch. Spacecraft attitude control and stabilization: Applications of geometric control theory to rigid body models. *IEEE Transactions on Automatic Control*, 29(4):321–331, 1984.

[21] Christopher I Byrnes and Alberto Isidori. On the attitude stabilization of rigid spacecraft. *Automatica*, 27(1):87–95, 1991.

[22] James Richard Forbes and Christopher John Damaren. Geometric approach to spacecraft attitude control using magnetic and mechanical actuation. *Journal of Guidance, Control, and Dynamics*, 33(2):590–595, 2010.

[23] Jean-François Trégouët, Denis Arzelier, Dimitri Peaucelle, Christelle Pittet, and Luca Zaccarian. Reaction wheels desaturation using magnetorquers and static input allocation. *IEEE Transactions on Control Systems Technology*, 23(2):525–539, 2015.

[24] Marco Lovera and Alessandro Astolfi. Global magnetic attitude control of inertially pointing spacecraft. *Journal of guidance, control, and dynamics*, 28(5):1065–1072, 2005.

[25] Fabio Celani. Robust three-axis attitude stabilization for inertial pointing spacecraft using magnetorquers. *Acta Astronautica*, 107:87–96, 2015.

[26] Carlo Arduini and Paolo Baiocco. Active magnetic damping attitude control for gravity gradient stabilized spacecraft. *Journal of Guidance, Control, and Dynamics*, 20(1):117–122, 1997.

[27] Christopher J Damaren. Hybrid magnetic attitude control gain selection. *Proceedings of the Institution of Mechanical Engineers, Part G: Journal of Aerospace Engineering*, 223(8):1041–1047, 2009.

[28] Giulio Avanzini and Fabrizio Giulietti. Magnetic detumbling of a rigid spacecraft. *Journal of guidance, control, and dynamics*, 35(4):1326–1334, 2012.

[29] G Avanzini, EL de Angelis, and F Giulietti. Spin-axis pointing of a magnetically actuated spacecraft. *Acta Astronautica*, 94(1):493–501, 2014.

[30] Tiziano Pulecchi and Marco Lovera. Attitude control of spacecraft with partially magnetic actuation. *IFAC Proceedings Volumes*, 40(7):609–614, 2007.

[31] Fabrizio Giulietti, Alessandro A Quarta, and Paolo Tortora. Optimal control laws for momentum-wheel desaturation using magnetorquers. *Journal of guidance, control, and dynamics*, 29(6):1464–1468, 2006.

[32] Jean-François Trégouët, Denis Arzelier, Dimitri Peaucelle, and Luca Zaccarian. Static input allocation for reaction wheels desaturation using magnetorquers. *IFAC Proceedings Volumes*, 46(19):559–564, 2013.

[33] Kirill A Antipov and Alexey A Tikhonov. On the spacecraft attitude stabilization in the orbital frame. *Theoretical and Applied Mechanics*, 39(2):127–163, 2012.

[34] Erik A Hogan and Hanspeter Schaub. Three-axis attitude control using redundant reaction wheels with continuous momentum dumping. *Journal of Guidance, Control, and Dynamics*, 38(10):1865–1871, 2015.

[35] BT Costic, DM Dawson, MS De Queiroz, and V Kapila. Quaternion-based adaptive attitude tracking controller without velocity measurements. *Journal of Guidance, Control, and Dynamics*, 24(6):1214–1222, 2001.

[36] Elena Panteley and Antonio Loria. Global uniform asymptotic stability of cascaded non-autonomous nonlinear systems. In *Control Conference (ECC), 1997 European*, pages 973–978. IEEE, 1997.

[37] Giulio Avanzini, Emanuele L de Angelis, and Fabrizio Giulietti. Acquisition of a desired pure-spin condition for a magnetically actuated spacecraft. *Journal of Guidance, Control, and Dynamics*, 36(6):1816–1821, 2013.

[38] Davide Bruzzi, Paolo Tortora, Fabrizio Giulietti, and Piero Galeone. European student earth orbiter: Esas educational microsatellite program. 2013.

[39] A Craig Stickler and KT Alfriend. Elementary magnetic attitude control system. *Journal of spacecraft and rockets*, 13(5):282–287, 1976.

[40] Jefferson R Chaurais, Henrique C Ferreira, João Y Ishihara, and Renato A Borges. Attitude control of an underactuated satellite using two reaction wheels. *Journal of Guidance, Control, and Dynamics*, 38(10):2010–2018, 2015.

[41] Panagiotis Tsiotras and Jihao Luo. Control of underactuated spacecraft with bounded inputs. *Automatica*, 36(8):1153–1169, 2000.

[42] Hirohisa Kojima. Stabilization of angular velocity of asymmetrical rigid body using two constant torques. *Journal of guidance, control, and dynamics*, 30(4):1163–1168, 2007.

[43] Pascal Morin and Claude Samson. Time-varying exponential stabilization of a rigid spacecraft with two control torques. *IEEE Transactions on Automatic Control*, 42(4):528–534, 1997.

[44] Congying Han and Alexandre N Pechev. Underactuated satellite attitude control with two parallel cmgs. In *Control and Automation, 2007. ICCA 2007. IEEE International Conference on*, pages 666–670. IEEE, 2007.

[45] Congying Han and Alexandre N Pechev. Time-varying nonlinear designs for underactuated attitude control with two reaction wheels. In *ASME 2008 9th Biennial Conference on Engineering Systems Design and Analysis*, pages 653–657. American Society of Mechanical Engineers, 2008.

[46] Hariharan Krishnan, Mahmut Reyhanoglu, and Harris McClamroch. Attitude stabilization of a rigid spacecraft using gas jet actuators operating in a failure mode. In *Decision and Control, 1992., Proceedings of the 31st IEEE Conference on*, pages 1612–1617. IEEE, 1992.

[47] Nadjim Mehdi Horri and Stephen Hodgart. Attitude stabilization of an underactuated satellite using two wheels. In *Aerospace Conference, 2003. Proceedings. 2003 IEEE*, volume 6, pages 6_2629–6_2635. IEEE, 2003.

[48] Hariharan Krishnan, Mahmut Reyhanoglu, and Harris McClamroch. Attitude stabilization of a rigid spacecraft using two control torques: A nonlinear control approach based on the spacecraft attitude dynamics. *Automatica*, 30(6):1023–1027, 1994.

[49] Daniele Casagrande, Alessandro Astolfi, and Thomas Parisini. Global asymptotic stabilization of the attitude and the angular rates of an underactuated non-symmetric rigid body. *Automatica*, 44(7):1781–1789, 2008.

[50] Haichao Gui, Lei Jin, and Shijie Xu. Attitude maneuver control of a two-wheeled spacecraft with bounded wheel speeds. *Acta Astronautica*, 88:98–107, 2013.

[51] A Behal, D Dawson, E Zergeroglu, and Y Fang. Nonlinear tracking control of an underactuated spacecraft. *Journal of Guidance, Control, and Dynamics*, 25(5):979–985, 2002.

[52] TB Ake, BF Class, BA Roberts, JW Kruk, WP Blair, HW Moos, and FUSE Operations Team. Recovery of fuse attitude control with two reaction wheels and magnetic torquer bars. In *Bulletin of the American Astronomical Society*, volume 34, page 671, 2002.

[53] Clemens E Tillier and Brij N Agrawal. Yaw steering for a leo satellite using any two of three reaction wheels. In *IAF, International Astronautical Congress, 51 st, Rio de Janeiro, Brazil*, 2000.

[54] Haichao Gui, Lei Jin, and Shijie Xu. Global feedback control for attitude maneuvers of a spacecraft by two reaction wheels. In *AIAA/AAS Astrodynamics Specialist Conference*, page 5016, 2012.

[55] Sungpil Kim and Youdan Kim. Sliding mode stabilizing control law of underactuated spacecraft. In *AIAA Guidance, Navigation and Control Conference and Exhibit*, 2000.

[56] Hariharan Krishnan, N Harris McClamroch, and Mahmut Reyhanoglu. Attitude stabilization of a rigid spacecraft using two momentum wheel actuators. *Journal of Guidance, Control, and Dynamics*, 18(2):256–263, 1995.

[57] Panagiotis Tsiotras and James M Longuski. Spin-axis stabilization of symmetric spacecraft with two control torques. *Systems & Control Letters*, 23(6):395–402, 1994.

[58] Panagiotis Tsiotras, Martin Corless, and JM Longuski. A novel approach to the attitude control of axisymmetric spacecraft. *Automatica*, 31(8):1099–1112, 1995.

[59] Panagiotis Tsiotras and Jihao Luo. A reduced-effort control law for underactuated rigid bodies. In *Decision and Control, 1996., Proceedings of the 35th IEEE Conference on*, volume 1, pages 495–496. IEEE, 1996.

[60] Panagiotis Tsiotras. Optimal regulation and passivity results for axisymmetric rigid bodies using two controls. *Journal of Guidance, Control, and Dynamics*, 20(3):457–463, 1997.

[61] Haijun Shen and Panagiotis Tsiotras. Time-optimal control of axisymmetric rigid spacecraft using two controls. *Journal of Guidance, Control, and Dynamics*, 22(5):682–694, 1999.

[62] In-Ho Seo, Henzeh Leeghim, Dong-Heon Lee, and Hyochoong Bang. Momentum transfer control of a spacecraft with two wheels by feedback linearization. In *Control, Automation and Systems, 2008. ICCAS 2008. International Conference on*, pages 175–180. IEEE, 2008.

[63] Frédéric Boyer and Mazen Alamir. Further results on the controllability of a two-wheeled satellite. *Journal of guidance, control, and dynamics*, 30(2):611–619, 2007.

[64] Xinsheng Ge and Liqun Chen. Optimal reorientation of underactuated spacecraft using genetic algorithm with wavelet approximation. *Acta Mechanica Sinica*, 25(4):547–553, 2009.

[65] Jason S Hall, Marcello Romano, and Roberto Cristi. Quaternion feedback regulator for large angle maneuvers of underactuated spacecraft. In *American Control Conference (ACC), 2010*, pages 2867–2872. IEEE, 2010.

[66] Dirk Aeyels and Marek Szafranski. Comments on the stabilisability of the angular velocity of a rigid body. *Systems & Control Letters*, 10(1):35–39, 1988.

[67] Sungpil Kim and Youdan Kim. Spin-axis stabilization of a rigid spacecraft using two reaction wheels. *Journal of Guidance, Control, and Dynamics*, 24(5):1046–1049, 2001.

[68] Congying Han, Jian Guo, and Alexandre Pechev. Nonlinear h based underactuated attitude control for small satellites with two reaction wheels. *Acta Astronautica*, 104(1):159–172, 2014.

[69] F. Giulietti G.Avanzini, L. Berardo and E.A. Minisci. Optimal rotation sequences in presence of constraints on admissible rotation axes. *Journal of Guidance, Control, and Dynamics*, Vol.34(No. 2):554–563, 2011.

[70] Michael S Branicky. Studies in hybrid systems: Modeling, analysis, and control. Technical report, DTIC Document, 1995.

[71] Michael S Branicky. Multiple lyapunov functions and other analysis tools for switched and hybrid systems. *IEEE Transactions on automatic control*, 43(4):475–482, 1998.

[72] Hassan K Khalil. *Nonlinear Systems,Third Edition*. Prentice-Hall, New Jersey, 2001.

[73] Raymond A DeCarlo, Michael S Branicky, Stefan Pettersson, and Bengt Lennartson. Perspectives and results on the stability and stabilizability of hybrid systems. *Proceedings of the IEEE*, 88(7):1069–1082, 2000.